CHALMERS
UNIVERSITY OF TECHNOLOGY

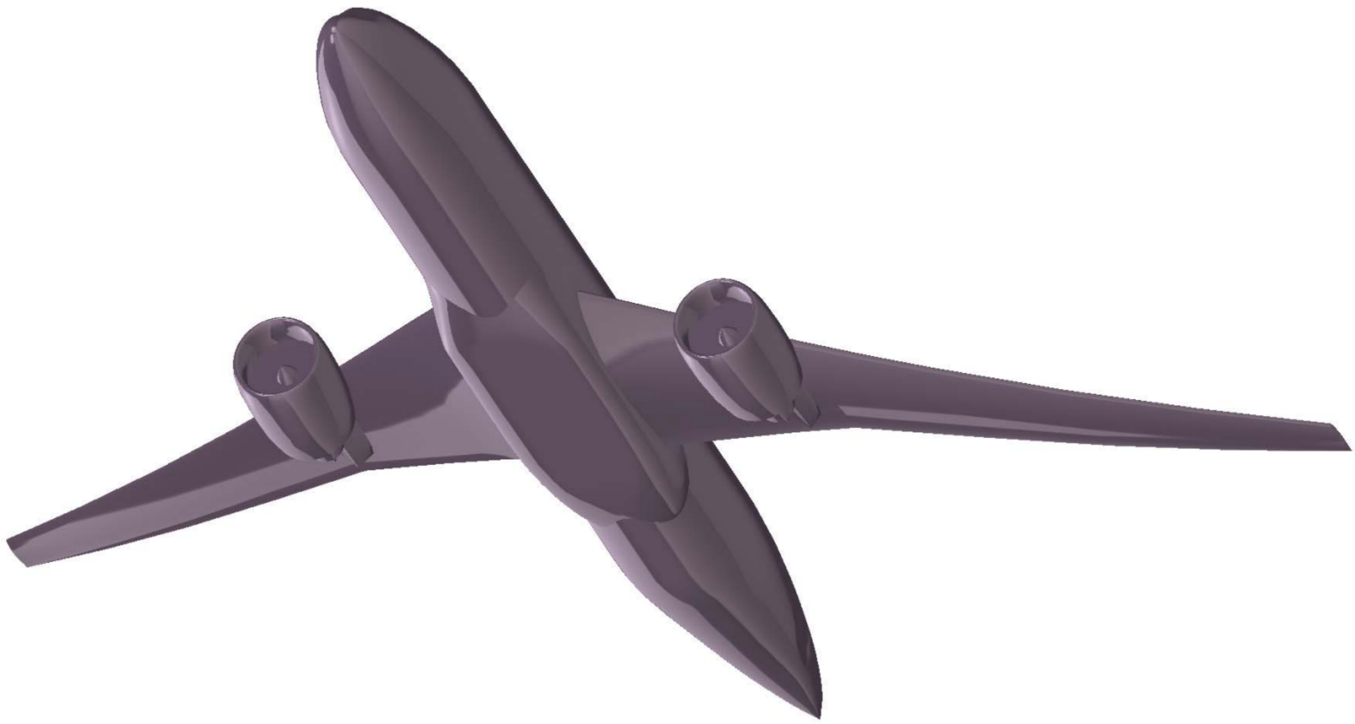

Fluid-structure interaction of NASA High Speed Common Research Model

Master's thesis in Solid and Fluid Mechanics

Adrià Hueso

DEPARTMENT OF MECHANICS AND MARITIME SCIENCES
CHALMERS UNIVERSITY OF TECHNOLOGY
Gothenburg, Sweden 2022
www.chalmers.se

Master's thesis 2022

Fluid-structure interaction of NASA High Speed Common Research Model

CHALMERS
UNIVERSITY OF TECHNOLOGY

Department of Mechanics and Maritime Sciences
Division of Fluid Dynamics
Chalmers University of Technology
Gothenburg, Sweden 2022

Fluid-structure interaction of NASA High Speed Common Research Model
Adrià Hueso

Supervisor: Massoud Tatar, Department of Fluid Dynamics
Examiner: Huadong Yao, Department of Fluid Dynamics

Master's Thesis 2022
Division of Fluid Dynamics
Department of Mechanics and Maritime Sciences
Chalmers University of Technology
SE-412 96 Gothenburg
Telephone +46 31 772 1000

Cover: High Speed Common Research Model.

Typeset in LaTeX
Printed by Chalmers Reproservice
Gothenburg, Sweden 2022

Fluid-structure interaction of NASA High Speed Common Research Model
Adrià Hueso
Department of Fluid Dynamics
Chalmers University of Technology

Abstract

In recent years, the computational study of fluid-structure interaction has become increasingly important. This is due to the increased demand for more efficient aircraft designs without compromising the integrity of the aircraft. The concept of aeroelasticity is essential to the design process of aircraft to ensure that instabilities leading to a catastrophic scenario do not occur.

The interaction between a flexible structure and the aerodynamic forces acting on it is studied in this thesis. Especially, the study is carried out for full-scale aircraft at transonic Mach number. In this critical speed regime, the aeroelastic instabilities might commence. And even more so with the implementation of UHBPR nacelles, which have a great effect on the pressure distribution over the wing surface.

The model studied is the Common Research Model developed (CRM) by NASA, available in open source on their website [1]. An initial preparation has been necessary in SolidWorks to repair the CAD and then use it in the CFD tools. For the CFD simulation of the flow, ANSYS Fluent is used. The turbulence model used in the simulations is k-omega SST. ANSYS Mechanical (static structural and transient structural) is used to determine the static and dynamic response of the structure under the pressure loads imposed by the flow. For structural analysis, Finite Element Method (FEM) is used. The CFD and structure solvers are coupled in Workbench through the System Coupling module.

Several results are provided: verification of the CRM's aerodynamics; CRM wing tip deformations (one-way FSI) for the full-scale model and the 1/21 scale model as well as a comparison of the aerodynamic forces between them; flutter deformation and frequency (two-way FSI) for the AGARD445.6 wing (the benchmark case).

The study is useful for a better understanding of the CRM behaviour. In this way, a computational model is obtained that can be used for future comparison with wind tunnel experiments. For future work, it would be interesting to take into account the internal structure of the wing and fuselage to obtain more realistic results, although the high computational costs limit this type of study.

Keywords: Aeroelasticity, Common Research Model, Fluid-Structure Interaction, Transonic, Partitioned Approach, Dynamic mesh, Deformation.

Acknowledgements

First of all, I have to thank my family for their support, but especially my parents, who made it possible for me to do my Master's thesis abroad.

I would like to thank Professor Huadong Yao for giving me the opportunity to be part of this project group to carry out this master's thesis, which has helped me a lot to increase my knowledge in this field, in which I am really interested and I want to keep learning in the future.

Thanks to Philip van Hoorn for his contribution in providing the necessary simulation files and other help as a co-supervisor.

Finally, to Massoud Tatar, to whom I owe infinite thanks. Countless hours have been dedicated to helping me learn everything I need to know (and much more) in this field. I will be eternally grateful!

Without all those mentioned above, this thesis would not have been possible. Thank you all very much for everything.

Adrià Hueso, Gothenburg, 12/9/2022

List of Acronyms

AoA	Angle of Attack
CAD	Computational Aided Design
CD	Drag Coefficient
CFD	Computational Fluid Dynamics
CL	Lift Coefficient
CP	Pressure Coefficient
CRM	Common Research Model
CSD	Computational Structural Dynamics
FEA	Finite Element Analysis
FEM	Finite Element Method
FSI	Fluid Structure Interaction
PDE	Partial Differential Equation
RANS	Reynolds-Averaged Navier-Stokes
SST	Shear Stress Transport
WB	Wing-Body
WBPN	Wing-Body-Pylon-Nacelle

Contents

List of Figures

List of Tables

1
Introduction

1.1 Background

To tackle the environmental pollution problems, today the tendence of long-range aircraft technology is to adopt ultrahigh bypass ratio (UHBPR) engine nacelles. However, this type of nacelle poses new challenges on obtaining efficient aerodynamics near the nacelle walls. Because a UHBPR nacelle has a much larger diameter, its large size significantly constrains the flow between the wing and itself, leading to asymmetry pressure distribution near the nacelle. This asymmetry flow feature could deteriorate the aerodynamic efficiency to a large extent if it is not well controlled.

There are many things to be taken into account in the incorporation of these new, much larger nacelles. In particular, this master thesis has focused on the study of the fluid-structure interaction of the Common Research Model (CRM). Therefore, for this study it is required to enter into the fields of Computer-Aided Design (CAD), Finite Element Analysis (FEA) and Computational Fluid Dynamics (CFD).

However, this is an initial study, where the internal structure of the different components is not taken into account. To do that, more computational resources are needed, as well as more time.

1.2 Aim

In the project, different configurations of Common Research Model (CRM) will be studied using Computational Fluid Dynamics simulation (CFD). Particularly, the different configurations will be:

- Wing-Body (WB)
- Wing-Body-Pylon-Nacelle (WBPN)

The plan is to analyse the aerodynamic performance parameters (drag and lift coefficients, etc.) at several angles of attack (AoAs) at the cruise condition of Mach=0.85. Subsequently, a fluid-structure interaction analysis will be done. As mentioned before, due to the high computational cost, a One-way FSI will be performed.

On the other hand, in order to demonstrate the abilities and creating a framework of Two-way study, it has been carried out a benchmark study related to AGARD445.6. In it, the oscillatory behaviour of the wing displacement at different speeds will be studied in order to understand the flutter under specific conditions. The aim of this part of the study will be to be able to confirm and validate the results with globally accepted scientific references, thus leaving the work ready for further research on the different parameters and results obtained. As mentioned above, the initial objective of this part of the thesis is to understand the functioning of this type of analysis in order to carry it out in the future, if the required computational resources are available, by applying it to the Common Research Model (CRM).

1.3 Scope and limitations

The scope of this project is to carry out fluid-structure interaction simulations in which the airflow passes through the CRM under specific flight conditions. Thus, to understand the behaviour of the Common Research Model. In addition, various aerodynamic coefficients at different Angles of Attack (AoA) are also studied.

As for the limitations of the project, there are many. First of all, the geometry provided by the NASA website is Open Source, and it is necessary to put in some effort. It is not "*plug and play*". A multitude of different repairs that appear in the geometry are necessary, although it may depend on the software used.

On the other hand, most of the studies have been carried out using the Chalmers Cluster. However, for the software used (Ansys Workbench) there was a problem in the structural module. Therefore, the FSI studies were very limited, since in order to carry out the Two-way FSI study of the CRM, a mesh of a large number of cells is necessary, which is not affordable for a local computer. For this reason, the study remained a CRM One-way FSI study. It should also be noted that the internal structure of the model has not been taken into account. However, this cannot be considered a major limitation either, because although it would be a very interesting challenge, the real objective is to obtain a computational model to compare the results with those obtained experimentally in the wind tunnel. Such a model is completely filled, so the internal structure should not be taken into account.

Due to the limitation for the Two-way, a Benchmark study has been carried out as a framework and demonstration of the procedure that would have to be carried out with the CRM. The AGARD445.6 wing was chosen for this demonstration. In addition, the study is also carried out under transonic flow conditions, so that the problems we would encounter for the CRM problem would be similar.

2

Theoretical background

2.1 Aeroelasticity overview

The term of aeroelasticity is commonly defined as the science which studies the mutual interaction between aerodynamic and elastic forces, and the effect of this interaction on airplane design. If the airplane structures were completely rigid, the aeroelastic problems would not exist. In these days, one of the biggest challenges is to reduce the aircraft's own weight, so research into new materials in this field is at the forefront. Composite materials have played a major part in weight reduction. These materials tend to have a lower stiffness than those traditionally used, so they have a more elastic behaviour. This behaviour highlights the importance of studying aeroelastic phenomena in order to avoid catastrophic scenarios.

The interesting part of this phenomena is related to the additional aerodynamic forces which are induced by the structural flexibility. Consequently, the additional aerodynamic forces can produce additional structural deformations which will became greater aerodynamic forces. These interactions may tend to become a damped solution if it is a stable system or to diverge and, in the worst case scenario, to destroy the structure. [2]

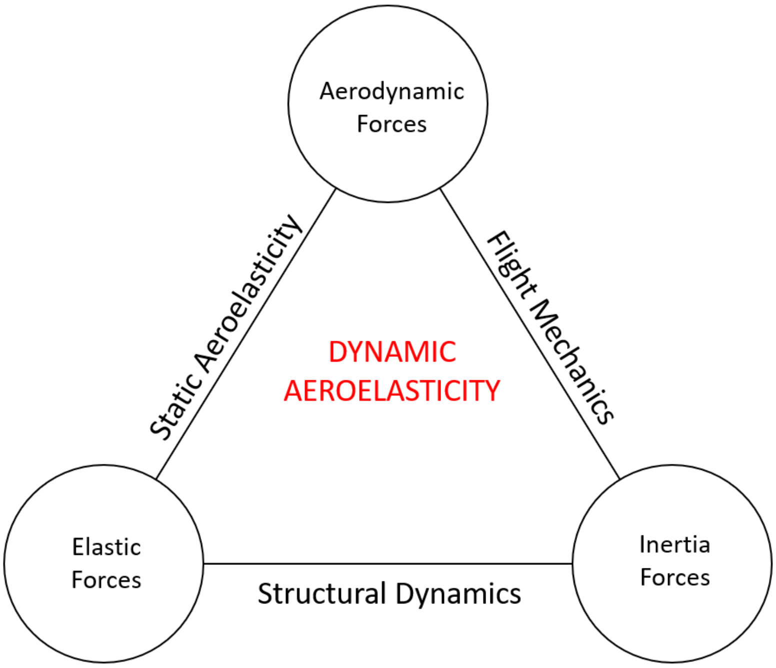

Figure 2.1: Aeroelastic triangle of forces. Source: Own

Aeroelastic phenomena is divided according to Figure 2.1. The vertexes of the triangle represent the forces from specific areas (aerodynamic, elastic and inertial). Then, the sides of the triangle are representing the relationship among these pair of forces. Mechanical vibrations are caused by the combination of elastic and inertia forces (structural dynamics) whereas the dynamic stability is composed of the aerodynamic and inertia forces (flight mechanics). Finally, the combination of aerodynamic and elastic forces excluding the inertia forces represents the unidirectional deformation of the structure (static aeroelasticity). When inertial forces are included in the latter, we are faced with the interference of all groups result in the dynamic elastic phenomena.

2.1.1 Flutter: Influence of Aeroelastic Phenomena on Design

The aeroelastic problems in current high-speed aircraft have very important effects in the design of the structure and mass distribution. Flutter is perhaps the most studied phenomena in aeroelasticity on the design of high-speed aircrafts. There are many types of flutter phenomena.

On the one hand, the classical type of flutter is associated with potential flow. For the non-classic flutter, could be involve separated flow, periodic breakaway and flow reattachment, stalling conditions and different time-lag effects between aerodynamic forces and displacement. Some of the most common preventive measures to avoid undesired scenarios are increased rigidity or the decreased coupling adjusting the mass distribution, or a combination of both. It is important to taking into account the torsional stiffness, so it is the most important stiffness parameter in the considerations of flutter. For that reason it is common to control the wing skin thickness. Moreover, aspect ratio and wing planform have also important effects on flutter phenomena.

Flutter considerations can affect the design of the control surface in defining the aerodynamic and mass balance, the location of the hinges and the degree of irreversibility required in the actuation system. [2]

2.2 Fluid Structure Interaction

This chapter describes the meaning of FSI. Fluid-structure interaction relates to problems concerning the interaction of fluids around a structure to study its behaviour. These types of problems are seen in various field of industry, for example in aeronautics, civil engineering, turbomachinery, and they are also researched in computational fluid dynamics. [3]

FSI is concerned with the coupled dynamics of structures in contact with a fluid. As sketched in Figure 2.2, the basic mechanism of fluid and structure coupling may be described as follows: the flow effect generates the motion of the structure at the interface zone, which in turn induces a fluctuation in the pressure and/or viscous forces; the loading applied to the fluid–structure interface subsequently changes the structure motion. [4]

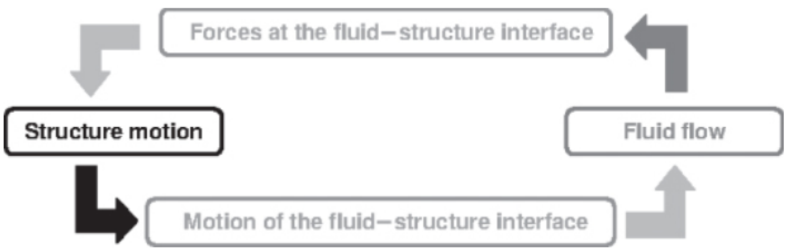

Figure 2.2: Fluid–structure interaction: coupling mechanism. Source: [4]

The FSI concept is considered critical for the design of many products. The product performance can be affected by not accurately accounting for the effects of a fluid on a solid or vice versa. Consequently, the final product may experience unexpected or undesirable effects very important for the proper functioning or even for the safety.

Depending on the degree of physical coupling between the fluid and solid and the level of fidelity needed, different approaches can be studied. In the case of this study, the deformations must be taken into account. Hence, the fluid and structural simulations are coupled to transfer data between the solvers for either a one-way or two-way coupled simulation. [5]

2.2.1 Methods

In general, Fluid-Structure Interaction problems are multiphysics problems which are very difficult to solve by analytical approach. Therefore, they are to be analysed either by using numerical simulations or experiments. Advanced discretization methods and availability of modern softwares in fields of computational fluid dynamics (CFD) and computational structural dynamics (CSD) have made this numerical solution possible.

There are mainly two approaches for solving FSI problems. On the one hand, COMSOL Multi-physics is one of the most known softwares which uses the monolithic approach. On the other hand, for the partitioned approach, there are popular softwares as ANSYS, ABAQUS, among others. [6]

These two approaches are explained hereafter.

2.2.1.1 Monolithic approach

The monolithic approach treats the fluid and structure dynamics in the same mathematical framework to form a single system equation for the entire problem, which is solved simultaneously by a unified algorithm. [7][8]

The interface conditions of fluid and structure are implicit in this solution approach. This process is better and more accurate for a multi-physics problem, but it may demand more resources and computational memory to develop and maintain such a specialized algorithm. The mesh is connected here by non-conforming mesh methods. The non-conforming mesh methods consider the interface conditions as physical boundary conditions, which treat the interface location as part of the solution, and requires meshes that conform to the interface. [9][6]

The following Figure 2.3 shows the work flow of the monolithic approach:

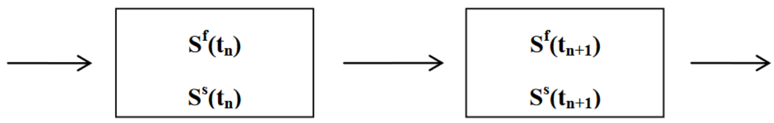

Figure 2.3: Monolithic approach. Source: [6]

2.2.1.2 Partitioned approach

The partitioned approach is another way to solve Fluid-structure interaction problems which treats the fluid and the structure as two computational fields which can be solved separately with their respective mesh discretization and numerical algorithm. The interface conditions are used explicitly to communicate information between the fluid and structure solutions. In short, sub programs are solved individually so that the structural solution does not change at the same time when fluid flow solution is computed.

A motivation of this approach is to combine the fluid and structural algorithm and to save computational time. Hence, a partitioned method can be used to compute Fluid-structure interaction problems with sophisticated fluid and structural physics [2]. A conforming mesh method is mainly used here to connect the mesh.

The following Figure 2.4 shows the work flow of the partitioned approach:

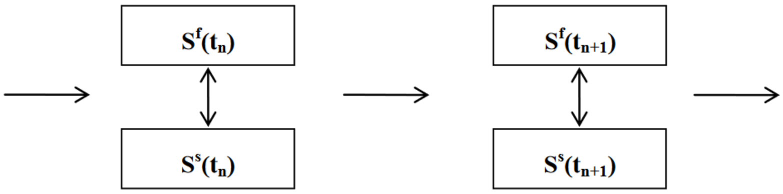

Figure 2.4: Partitioned approach. Source: [6]

2.2.2 One-way coupling

In this type of coupling, one field that has to be solved is fluid dynamics, the other is structure dynamics. At the boundary between fluids and solids, the fluid-structure interface, information for the solution is shared between the fluid solver and structure solver. The information exchanged is dependent on the coupling method. For one-way coupling calculations, only the fluid pressure acting at the structure is transferred to the structure solver. [10]

A coupling is said to be one-way if the motion of a fluid flow is affected by structural deformation and vice versa. In this coupling method, fluid flow is calculated first up to the desired convergence. Afterwards, the resulting fluid flow calculation is interpolated to the structural model at the interface. Then, the structural model calculation is iterated until the desired convergence is achieved. [6]

In other words, for one-way problems, only the pressure generated by the fluid at the structure is transferred to the structural solver. In the Figure 2.5 is described the work flow for one-way coupled.

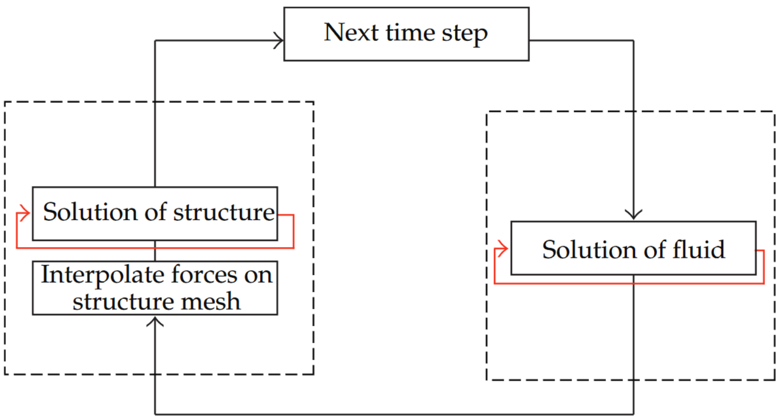

Figure 2.5: One-way coupling workflow. Source: [10]

2.2.3 Two-way coupling

For two-way problems, the dynamics are slightly different.The displacement of the structure is also transferred to the fluid solver at each coupling step. At each time step, the converged solution calculated in the flow field provides the forces acting on the structure body. Thereupon, the forces received on the fluid-structure interface are interpolated to the structural mesh. The response of the structure to the loads from the fluid flow represents a displacement of the structural grid nodes. Consequently, the fluid mesh is deformed according to the structure deformation and the displacement is interpolated to the fluid grid. This process constitutes one complete loop of the simulation. Afterwards, another loop is launched.

In the Figure 2.6 is described the work flow for two-way coupled.

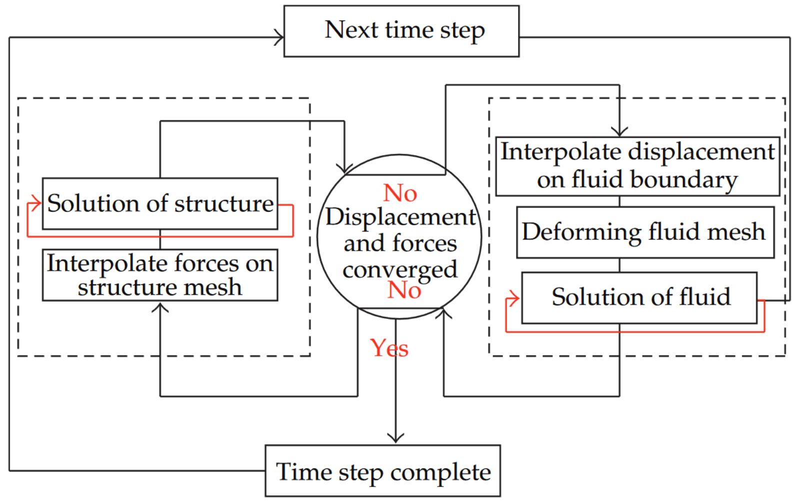

Figure 2.6: Two-way coupling workflow. Source: [10]

2.2.3.1 Dynamic mesh description

Dynamic meshing is a technique used to mesh a model that undergoes a change of shape during simulation. Depending on the technique used, it may consist of:

- Move boundaries or cell zones
- Deform cells
- Add/remove cells

Commonly, the dynamic mesh model is used when boundaries move rigidly (linear or rotating) with respect to each other. Although it can also be used when boundaries deform or deflect. The main difference compared to the fixed-mesh formulation is that the cell volume is now time-dependent.

For dynamic meshes, the equation 2.1 describes the integral form of the conservation equation for a general scalar, ϕ, on an arbitrary control volume, V, whose boundary is moving.

$$\frac{\partial}{\partial t}\int_V \rho\phi \mathrm{d}V + \int_{\partial V} \rho\phi\left(\vec{u} - \vec{u_g}\right)\mathrm{d}\vec{A} = \int_{\partial V} \Gamma\nabla\phi \mathrm{d}\vec{A} + \int_V S_\phi \mathrm{d}V \tag{2.1}$$

Where:
ρ is the fluid density
$\vec{u}$ is the flow velocity vector
$\vec{u}_g$ is the mesh velocity of the moving mesh

Γ is the diffusion coefficient
S_ϕ is the source term of ϕ

Here ∂V is used to represent the boundary of the control volume V.

Regarding the time step size selection, two time scales have to be considered where the smaller is dominant:

- Simulation
- Mesh deformation

An essential requirement with respect to dynamic meshing is that a boundary cannot move more than a single cell in each time step.

$$\nabla t < \frac{\nabla s}{v} \tag{2.2}$$

Hence, the maximum time step ∇t size has to be chosen based on:

- The length of the smallest cells ∇s
- The maximum expected velocity of the mesh v

There are various methods of dynamic mesh: Smoothing, Layering and Remeshing. Smoothing method has been used for the Two-way simulations of AGARD445.6 wing. Smoothing method consists in moving interior and boundary nodes to absorb the motion of a boundary, i.e., the number of nodes and connectivity does not change. One advantage of this method is that is available for all mesh types: try, tet, quad, hex, prism and poly meshes. For interior zones, three different smoothing methods are available:

- Spring-Based
- Diffusion-Based
- Linearly elastic solid smoothing

Diffusion-Based smoothing method has been chosen according to different advantages. For diffusion-based method, the mesh motion is governed by the diffusion equation (Eq. 2.3):

$$\nabla \cdot (\gamma \nabla \overrightarrow{u} = 0) \tag{2.3}$$

Where:
$\overrightarrow{u}$ is the mesh displacement velocity and γ is the diffusion coefficient

Fluent has two different formulation of the diffusion coefficient:

- Boundary distance formulation:

  $\gamma = \frac{1}{d^\alpha}$ where d is the normalized boundary and α is a user input parameter
- Cell volume formulation:

  $\gamma = \frac{1}{V^\alpha}$ where V is the normalized boundary and α is a user input parameter

Where:
$\alpha \geq 0$. Recommend range is between 0 and 2

$\alpha = 0$ gives $\gamma = 1$ and a uniform diffusion of the boundary motion into the interior of the mesh
A higher value of α reserves the mesh close the moving boundary better
$\alpha =$ 1-1.5 often works well for absorbing the motion with the "far field" mesh

In this method, the flow field must be initialized for obtaining values of d and V before previewing the mesh smoothing.

One of the reasons why this method was chosen was because Diffusion-based smoothing is generally more computationally costly than spring-based smoothing but tends to generate better quality meshes. [11]

Remeshing method has not been used. This method is usually used for situations where the boundary displacement is large compared to the size of the local cells, which causes the cell quality to deteriorate; thus, the mesh becomes invalid.

2.3 Governing equations in CFD

Continuity, Navier-Stokes and energy equations are the key governing equations that dictate the physics of fluid mechanics. [12]

Computational Fluid Dynamics is based mainly on the governing equations of fluid dynamics. [13] These governing equations represent mathematical statements of the conservation of laws of physics, which are the following:

- Conservation of mass.
- Second law of Newton: The rate of change of momentum equals the sum of the forces acting on the fluid.
- First law of thermodynamics: The rate of change of energy equals the sum of the rate of heat addition to the fluid and the rate of work done on the fluid.

After the governing equations are obtained, forms particularly suited for use in formulating CFD solutions will be delineated. The physical aspects of the boundary conditions and their appropriate mathematical statements will also be developed, since the appropriate numerical form of the physical boundary condition is strongly dependent on the particular mathematical form of the governing equations and numerical algorithm used. [13]

2.3.1 The continuity equation

This basic equation of aerodynamics is based in the fundamental principle in which the mass is conserved (i.e mass can be neither created nor destroyed).

Applying this principle in a finite control volume of a Volume V and Surface area S fixed in space, the resulting equation is [14]

$$\frac{\partial}{\partial t} \iiint\limits_V \rho \mathrm{d}V + \iint\limits_S \rho \mathrm{d}S = 0 \tag{2.4}$$

where the first integral over the control volume V is the time rate of change of mass inside the control volume and the second integral over the control surface S is the net flux of mass out of the control volume through the control surface. This is the integral form of the continuity equation.

Being the differential form:

$$\frac{\partial \rho}{\partial t} + \nabla \cdot (\rho V) = 0 \tag{2.5}$$

In both, ρ is the density of the flow and V is the flow velocity.[14]

2.3.2 The momentum equation

This equation is based on the second law of Newton (force = mass x acceleration). Applying this principle to a finite volume fixed in the space, we obtain

$$\frac{\partial}{\partial t} \iiint_V \rho V \mathrm{d}V + \iint_S (\rho V \mathrm{d}S) V = - \iint_S (\rho V) \mathrm{d}S + \iiint_V (\rho f) \mathrm{d}V + F_{viscous} \tag{2.6}$$

where the first integral is the time rate of change of momentum inside the control volume and the second integral is the net flux of momentum out of the control volume through the control surface.The terms on the right-hand side represent the force exerted on the fluid inside the control volume as it is momentarily flowing through the volume. Being f the body force per unit mass, and $F_{viscous}$ the net surface force due to friction.

The equation 2.6 can be expressed in terms of three scalar par-tial differential equations. [14]

2.3.3 The energy equation

This equation is based on *Energy is conserved; it can only change from one form to another form* which belongs to the first law of thermodynamics to the fluid flow. Applying this principle to a finite control volume fixed in space, we have

$$\begin{split}\iiint_V \dot{q} \rho \mathrm{d}V + \dot{Q}_{viscous} - \iint_S p V \mathrm{d}S + \iiint_V \rho (f V) \mathrm{d}V + \dot{W}_{viscous} = \\ \frac{\partial}{\partial t} \iiint_V \rho \left(e + \frac{V^2}{2} \right) \mathrm{d}V + \iint_S \rho \left(e + \frac{V^2}{2} \right) V \mathrm{d}S\end{split} \tag{2.7}$$

Being this last equation the integral form of the energy equation. Also, it can be described in partial differential equation form as

$$\begin{split}\frac{\partial}{\partial t} \left[\rho \left(e + \frac{V^2}{2} \right) \right] + \nabla \cdot \left[\rho \left(e + \frac{V^2}{2} \right) V \right] \\ = \rho \dot{q} - \nabla \cdot (pV) + \rho (f \cdot V) + \dot{Q}'_{viscous} + \dot{W}'_{viscous}\end{split} \tag{2.8}$$

where $\dot{Q}'_{viscous}$ and $\dot{W}'_{viscous}$ are the proper forms of the viscous terms. Equation 2.8 is a partial differential equation, which relates the flow field variables at a given point in space. [14]

2.4 Turbulence modeling

In daily life, the most of fluid flows that we encounter are turbulent. Typical examples are the flows around the cars, aircrafts, buildings, inside the engines, among others. Boundary layers and wakes generated around the bodies are turbulent. Hence, in most cases, the fluid flows studied will be turbulent. [15]

For turbulent flows, it is common to divide the variables in one time-averaged part U, independent of time (when the study is steady), and in one variable part u. Being $U = \bar{U} + u$.

It does not exist a unique definition of turbulence. It has a number of characteristic features such as:

- Irregularity
- Diffusivity
- Large Reynolds Numbers
- Three-Dimensional
- Dissipation
- Continuum

2.4.1 Turbulent scales

When the turbulent flows are studied, it should take into account that there are a wide range of scales. The larger scales are of the order of the flow geometries, e.g boundary layer thickness, with length scale L and velocity scale U. These scales extract the kinetic energy from the mean flow which has a time scale comparable to the larger scales.

The large scales kinetic energy is lost slightly to smaller with which are interacting large scales. The way by which the kinetic energy is transferred from largest scales to smaller scales is called cascade process. At smaller scales, the viscous stresses become too large and this kinetic energy is converted into internal energy. The dissipation (the transformation of kinetic energy into internal energy) is denoted by ε, which is energy per unit time and unit mass. It is important to highlight that the dissipation is proportional to the kinematic viscosity v by the fluctuating velocity gradient to the power of two. [15]

2.4.2 Vorticity/Velocity Gradient Interaction

In order to create the turbulence, it is essential the interaction between vorticity and velocity gradients. Disturbances are amplified and these disturbances, which still are laminar and organized and well defined in terms of physical orientation and frequency are turned into chaotic, three-dimensional and random fluctuations. [15]

2.5 RANS approach

The RANS equations are a reduced form of the general Navier-Stokes equations. In the RANS equations, the steady-state solution is decoupled from the time-varying fluctuations in the system, the latter of which will account for turbulence in different flow regimes.

The technique used to derive the RANS equations is called Reynolds decomposition. Reynolds averaging and Reynolds decomposition do not refer directly to a manipulation of the Reynolds number, but rather to an application of time averaging to the Navier-Stokes equations. Time averaging is often used to reduce complex systems of differential equations into simpler forms by partially or fully eliminating the time variable. [16]

2.5.1 The k-Omega Model

The k-omega ($k-\omega$) turbulence model is one of the most commonly used models to capture the effect of turbulent flow conditions. It belongs to the Reynolds-averaged Navier-Stokes (RANS) family of turbulence models where all the effects of turbulence are modeled.

It is a two-equation model. That means in addition to the conservation equations, it solves two transport equations (PDEs), which account for the history effects like convection and diffusion of turbulent energy. The two transported variables are turbulent kinetic energy (k), which determines the energy in turbulence, and specific turbulent dissipation rate (ω), which determines the rate of dissipation per unit turbulent kinetic energy. ω is also referred to as the scale of turbulence. [17]

The standard k - ω model is a Low Reynolds number model. Hence, it use to be used for flows with low Reynolds in which the boundary layer is thick and the viscous sub-layer can be resolved. In this way, this turbulence model is commonly used for near-wall treatment. It includes some other advantages as a better behaviour for complex boundary layer flows under adverse pressure gradients and separations. For instance, for external aerodynamics.

Other variations of this model are available, as for example, the one that is used for the present project, the K - ω SST, which includes some modifications to perform better under certain fluid flow conditions.

2.5.2 The k-Omega Shear Stress Transport (SST) Model

The term SST means Shear Stress Transport. The SST formulation is a combination between the k - ϵ and k - ω models. In order to avoid the problem of being sensitive to the inlet free-stream turbulence properties, the k - ϵ is used in the free-stream.

In this way, k - ω SST provides a better prediction of flow separation than most RANS models and also explains its good behaviour in adverse pressure gradients. It has the ability to account for the transport of the principal shear stress in adverse pressure gradient boundary layers.

As for the cons, the SST model produces some large turbulence levels in regions with large normal strain, like stagnation regions and regions with strong acceleration. This effect is much less pronounced than with a normal k-epsilon model though. [17] [18] [19]

2.6 Finite Element Method

The Finite Element Method is a numerical procedure for solving partial differential equations which describe the problem. The approach of this technique consists in represent a domain of interest in partial smaller parts, that is to say, finite elements. To obtain an approximate solution of the behaviour for the entire body we assemble the variations of the variables in the elements. In this way, the equations of each finite element are solved. One of the fields where this method is most used is in the study of elasticity, as in the case of this project, an aeroelastic study. In section 3.3 more detailed information about general equations is provided.

The physical problem typically involves the structure or structural component subjected to certain external loading condition. The idealization of the physical problem to the mathematical model requires certain assumptions that together leads to differential equations governing the mathematical model. The FEM is a numerical method, consequently it will be needed to reach an accuracy solution. If the objective numerical results are not founded, the numerical solution has to be repeated with refined solution parameters until a sufficient accuracy is obtained. For example, an option to obtain more accurate numerical results is to refine the mesh on the model. [20]

In this study, the solid part of the simulation has been performed using *ANSYS* Static Structural module. The principal elastic equation which is used is as follows:

$$\{\sigma\} = [E]\{\varepsilon\} \tag{2.9}$$

The normal strain ε is proportional to normal stress σ with Young's modulus E.

Therefore, Hooke's law for isotropic materials in compliance matrix form is given by:

$$\begin{bmatrix} \varepsilon_{xx} \\ \varepsilon_{yy} \\ \varepsilon_{zz} \\ \varepsilon_{yz} \\ \varepsilon_{zx} \\ \varepsilon_{xy} \end{bmatrix} = \frac{1}{E} \times \begin{bmatrix} 1 & -\nu & -\nu & 0 & 0 & 0 \\ -\nu & 1 & -\nu & 0 & 0 & 0 \\ -\nu & -\nu & 1 & 0 & 0 & 0 \\ 0 & 0 & 0 & 1+\nu & 0 & 0 \\ 0 & 0 & 0 & 0 & 1+\nu & 0 \\ 0 & 0 & 0 & 0 & 0 & 1+\nu \end{bmatrix} \begin{bmatrix} \sigma_{xx} \\ \sigma_{yy} \\ \sigma_{zz} \\ \sigma_{yz} \\ \sigma_{zx} \\ \sigma_{xy} \end{bmatrix} \tag{2.10}$$

The values of E and ν are specified in the Table 3.2

For a linear static structural analysis, the displacements {x} are solved for in the matrix equation below:

$$[K]\{x\} = F \tag{2.11}$$

Where it is assumed that:

- K is constant
    - Linear elastic material behavior is assumed
    - Small deflection theory is used
    - Some nonlinear boundary conditions may be included
- F is statically applied
    - No time-varying forces are considered
    - No inertial effects (mass, damping) are included

The development of the theory assumes that the solid material can be treated as a continuum. The length scale is significantly larger than the molecular scale so that properties are homogeneous, but small enough to be considered as infinitesimal from the mathematical point of view. [21]

Let the X coordinates denote the original location of a material particle. We can think of X as a label that is assigned to a given particle throughout the deformation history. This coordinate system is called the material coordinate system (or material frame). After a time t, the particle has been moved to another location $x = x(X, t)$. The coordinates are in the spatial coordinate system (or spatial frame). The spatial coordinate system is fixed in space, whereas the material coordinate system is fixed to the body. We can consider that the location and orientation of both coordinates systems are the same.

The vector pointing from the original location of a body point to its new location is the displacement vector, $u(X, t)$. Thus, the displacement provides the transformation from the material to the spatial frame, $x = X + u$.

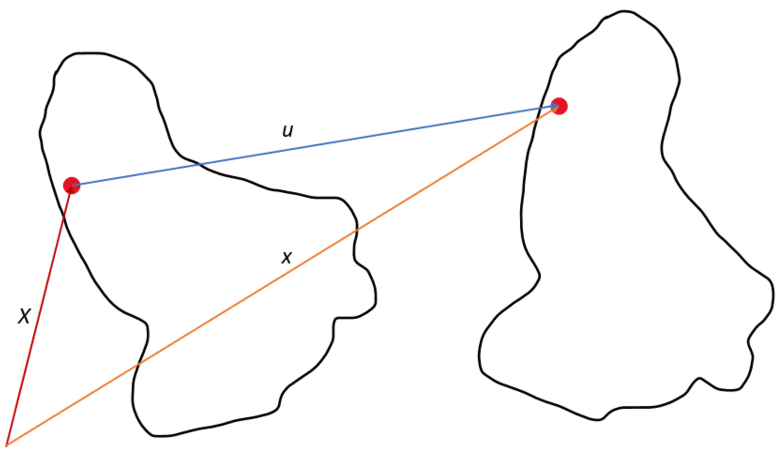

Figure 2.7: Relation between the material and spatial coordinates of a point. Source: Own Source

Although there is not a displacement on the body, there are local changes in the shape of the material, we refer to them as strains or stretches. These changes may consist of a change in the volume or shape of a small local domain. The deformations will cause internal forces in the material (stresses) and possibly even failure. To successfully describe the behavior of the material, the distortion must be described in a way that is independent of, for example, the motions of the rigid body. [21]

2.7 Transonic Flow

It is important to remark that the case of study is located in a transonic flow. For this reason, compressible-flow equations in their various forms are considered in order to predict the behaviour of airfoil sections in high sub- and supersonic flows.

It is a flow of air around an object at a certain velocity that generates both subsonic and supersonic regions. The specific range of velocities depends on the *critical* Mach number M_c. The value of the free-stream Mach number M_∞ at which flow somewhere on the surface first reaches $M = 1$ is called the *critical* Mach number M_c. [22]

Above the critical Mach number, the flow is mixed. As M_∞ increases progressively from low numbers to M_c, the aerodynamic characteristics of the airfoil section undergo progressive and smooth changes. On the other hand, as M_∞ increases progressively beyond M_c, a limited region in which the flow is supersonic develops from the point where the flow first became sonic and grows outward and downstream, terminating in a shock wave that is at first, normal to the surface. As M_∞ gets bigger, the shock wave tends to become stronger, longer and to move backwards. [22]

Finally, with a M_∞ value similar to M_c, both the upper and the lower shock waves reach the trailing edge. In this backward displacement, each shock wave reaches the rear axle at different time rates, the lower typically starting later and ahead of the upper, but moving faster and overtaking the upper before reaching the trailing edge.

2.7.1 Supercritical Airfoil

For transonic speeds, supercritical airfoils were designed to delay the appearance of wave drag. These type of airfoils are characterised by a low curvature all along the upper surface, a large leading edge radius and a larger camber in the aft section, as can be seen in Figure 2.8.

In comparison with conventional, supercritical airfoils have a shock wave much weaker than the shock on the NACA 6-series airfoils, postponing in this way the shock-induced boundary layer separation. In essence, the purpose of transonic airfoil design is to control the expansion of the flow to supersonic speed and its subsequent recompression.

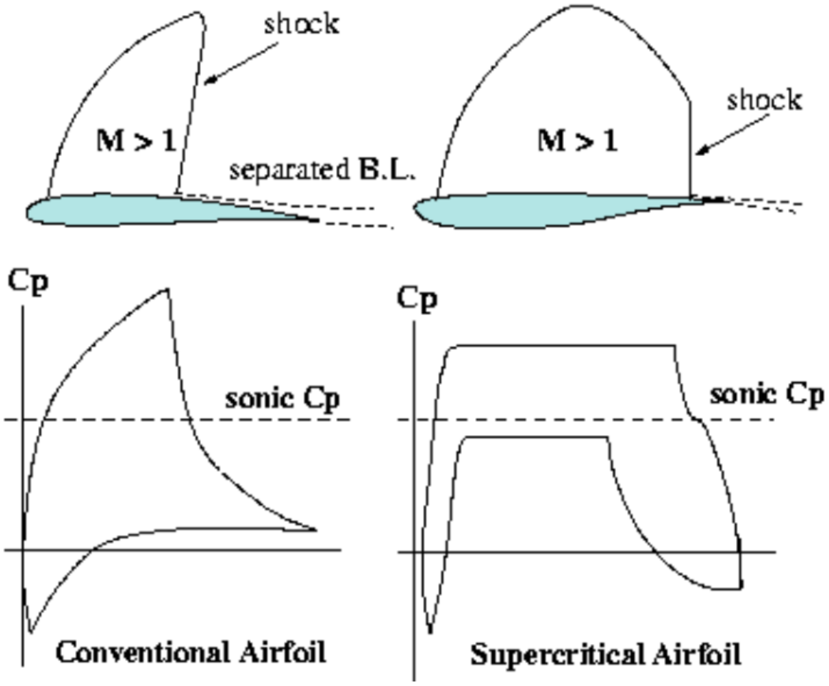

Figure 2.8: Conventional and supercritical airfoils at identical free-stream Mach number. Source: [23]

In Figure above is also shown for supercritical airfoils how the pressure distribution is "filled out" providing much more lift, although the shock formation is weaker compared to conventional airfoils. Moreover, related to the larger camber in the aft section, a high aft loading is formed.

As it has been described before, the CRM designed by NASA is the aim of this study. According to NASA [1], CRM should be based on a transonic transport configuration designed to fly at a cruise Mach number of M=0.85. Therefore, the outboard wing carries supercritical airfoil sections with about 1.5% camber as illustrated in the 2.9.

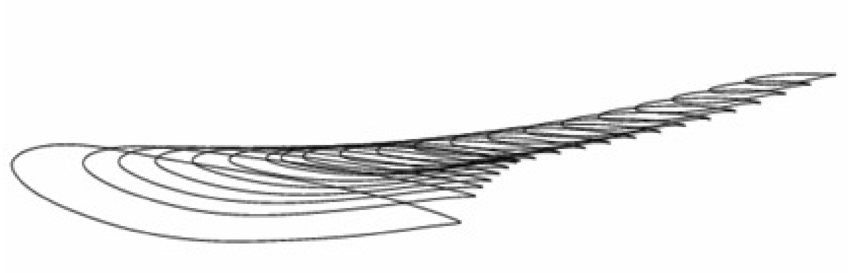

Figure 2.9: Airfoil Stack for the CRM Wing. Source: [1]

3

Methodology

The procedure for this study has been organised into three main parts, as described below:

3.1 Models of study

The different models studied have been provided by NASA, which are public and available in the Common Research Model website. Mainly, two models have been studied. First of all, in order to perform the validation study in a first stage, it was used the wing-body configuration, ignoring the pylon and nacelle. This model is presented in Figure 3.1.

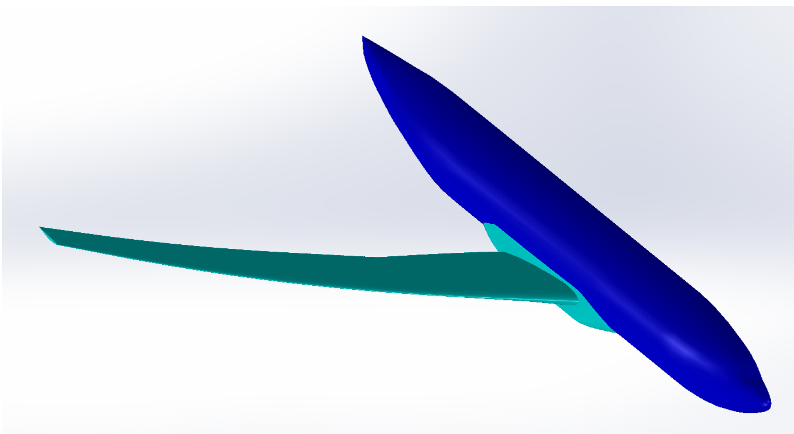

Figure 3.1: Wing-Body configuration model. Source: Own source

On the other hand, to go further and carry out a study closer to reality, the pylon and nacelle were added, as shown in Figure 3.2. In this way, it is possible to add a body-force model. The basic principle of this method consists of modeling the forces exerted by the fan blades of engine on the fluid instead of directly simulating the flow around the complete three-dimensional geometry. On the other hand, it is also possible to assign conditions to the surfaces that belong to the fan inlet and outlet.

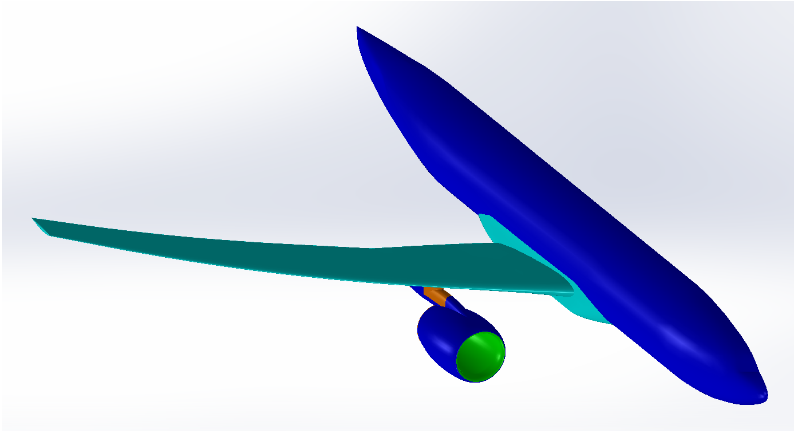

Figure 3.2: Wing-Body-Pylon-Nacelle configuration model. Source: Own source

3.2 CFD simulations using ANSYS Fluent

Initially, a case is developed to carry out a steady-state simulation in order to be able to get the results of different coefficients. Thus, this will be useful to compare the obtained results with different NASA workshops which are available on the website. In the first stage, the main aim is to compare the Drag, Lift, Moment and Pressure Coefficients with references.

Later, this steady-state simulation will be used to carry out the One-Way Fluid-structure interaction. This part is described in section 2.2.2. The solver adopted was for turbulent, specifically, for a transonic flow. This last concept has been introduced in the section 2.7. It is important to keep in mind that an important procedure in modeling of a fluid properly is the selection of accurate turbulent model. The accuracy of the turbulent model depends on many parameters mentioned in section 3.2.2. At high Reynolds number when the flow passes a slender body, a thin viscous boundary layer is formed. Actually, in practice, no flow has zero viscosity. But it is important to note that, if the boundary layer is not separated from the structure, one could use a non-viscous flow model and obtain acceptable results. However, according to the requirements of the project and based on the various references we can find on this particular aircraft model, the k-w SST turbulence model has been used. The details of this turbulence model can be reviewed in the section 2.5.2. Therefore, the Navier-Stokes equations described in section 2.3 are used.

Then, the first step to prepare the setup case, is to create the geometry of the fluid domain. As is shown in Figure 3.3, only half of the aircraft model is used, in order to save both computational resources and time.

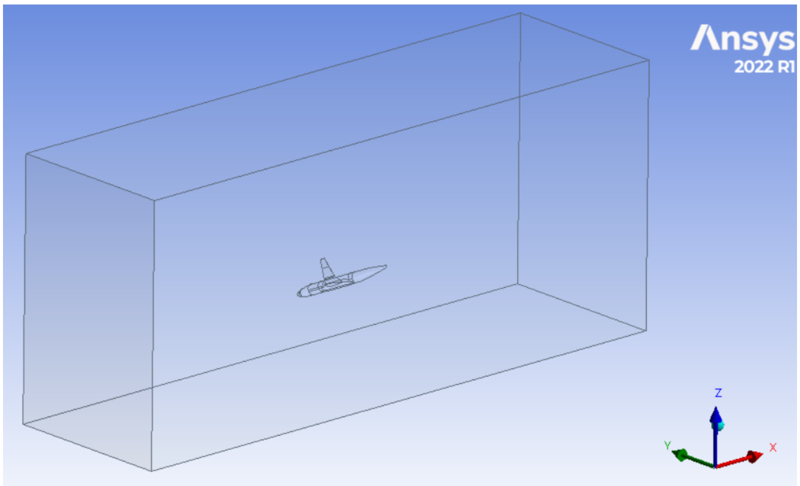

Figure 3.3: Fluid Domain. Source: Own source

3.2.1 CFD mesh

In order to mesh the block domain, an unstructured grid has been selected. It has been used the following meshers:

- Tetrahedral Mesher
- Prism Layer Mesher

Different controls in the ANSYS meshing option have been used in order to obtain good results. The mesh has been refined in specific places with the following controls:

- Edge control
- Surface control
- Volume control: Use of bodies of influence (Figure 3.4)

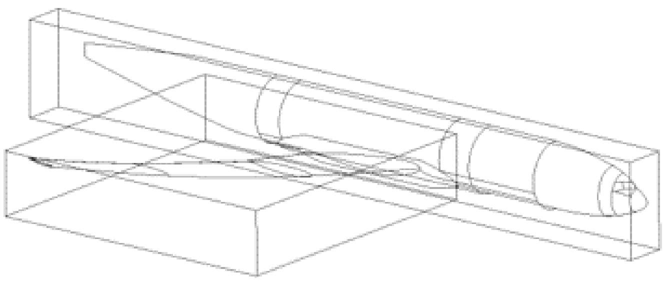

Figure 3.4: Use of body of influence in CRM. Source: Own source

The grids have been carried out with the commercial software named *ANSYS Meshing*. The grid is unstructured type as it has been mentioned before and has been done following the basic gridding guidelines by *ANSYS*. In Figure 3.5 it is shown the mesh used for the CRM.

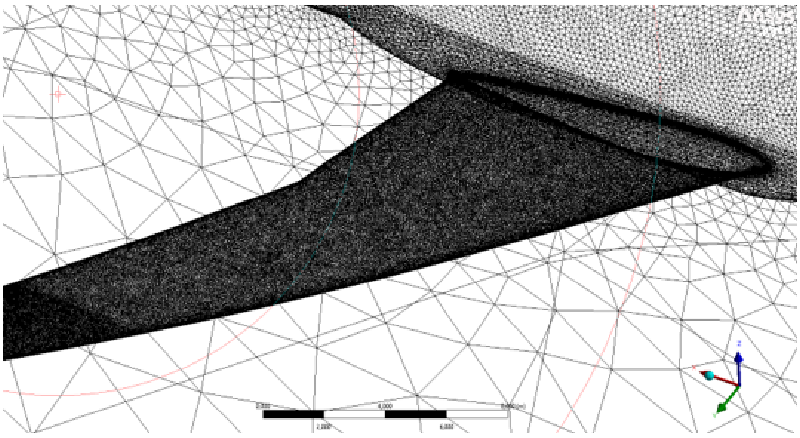

Figure 3.5: Common Research Model mesh. Source: Own source

Since the current master thesis has been carried out using the k-ω SST model, it is necessary to discuss some concepts. It is a model that does not make use of wall functions, so the dimensionless value of Y-Plus should be as close to 1 as possible.

In order to get the closest possible results to those given in the references that NASA itself has published, several tests have been carried out with different mesh refinements, until acceptable results have been achieved, always taking into account the computational cost. The computational cost in this project is really important, as the geometry is quite complex and with a lot of detail, so that sometimes, if you want to get results identical to the references, the computational cost is not affordable. In fact, the number of elements used was 10% compared to the different organisations, as there were not so many resources available.

Basic Gridding Guidelines:

- Boundary Layer Region

  $Y^+ \approx 1$

  First Layer Height $\Delta_1 = 0.000032m$

  Maximum Layers = 40

  Growth Rate = 1.2

- Domain size

  Element Number = 12M

  Poor mesh elements = 0

It has been taken into account that parameters as *skewness* or *orthogonal quality* within the acceptable ranges to consider the mesh as good quality.

In order to achieve more accurate flow modelling results in the interaction with the wing and fuselage structure, in addition to using the manual controls for surfaces and edges, the *body of influence* feature has been used to obtain better results in the area of interest without having to refine the entire domain. The same resource was also used to refine the volumetric mesh in the nacelle area, for the WBPN configuration.

3.2.2 Numerical Setup

3.2.2.1 Solver

In this section will be explained the main options that has been used to perform the simulations.

First of all, *Pressure-based solver* has been chosen. In *ANSYS Fluent*, two solver options are available; *Pressure-based solver* or *Density-based solver*. In these days, both solvers has been developed to solve and operate for a wide range of flow conditions, both incompressible and compressible. The pressure-based solver traditionally has been used for incompressible and slightly compressible flows. On the other hand, the density-based approach, was originally designed for high-speed compressible flows.

In both methods the velocity field is obtained from the momentum equations. In the density-based approach, the continuity equation is used to obtain the density field while the pressure field is determined from the equation of state.

In the pressure-based approach, the pressure field is extracted by solving a pressure or pressure correction equation which is obtained by manipulating continuity and momentum equations. [11]

3.2.2.2 Air properties

For the simulations, as far as the properties of the fluid, in this case Air, are concerned:

The density has been considered to follow the ideal gas law:

$$PV = nRT \tag{3.1}$$

The viscosity chosen was based on the operating temperature, following Sutherland's law:

$$\mu = \mu_0 \cdot \left(\frac{T_0 + C}{T + C}\right) \cdot \left(\frac{T}{T_0}\right)^{3/2} \tag{3.2}$$

Where:
μ = viscosity in centipoise at input temperature T
μ_0 = reference viscosity in centipoise at reference temperature T_0
T = input temperature in degrees Rankine
T_0 = reference temperature in degrees Rankine
C = Sutherland's constant

3.2.2.3 Boundary conditions

Regarding the operation conditions, in agreement with different NASA Workshops [24] has been considered:

- Reynolds Number = $5 \cdot 10^6$ (based on Mean Aerodynamic Chord)

- Mach Number = 0.85
- Temperature = 310.92 K

The properties of each zone in the block domain are described in the Table 3.1 below:

Boundary Conditions	
Zone	Type
farfield	pressure-far-field
sym	symmetry
fuselage	no-slip wall
wing	no-slip wall

Table 3.1: Boundary conditions in Fluent

3.3 FEA simulations using ANSYS Mechanical

As mentioned before, the model of study is the Common Research Model developed by NASA. Different models are shown in section 3.1. Based on the available literature on materials used in industry, Aluminium Alloy has been chosen for the deformation analysis of the model. Aluminium Alloy is the most-used metal in the aerospace engineering. The material properties are shown below in table 3.2.

The ANSYS solver uses Newton-Raphson method to minimize the overall energy of the system. This minimum energy is known as the static equilibrium of the structure due to interaction with external forces (in this project, the external forces are the the presure). [25]

Table 3.2: Properties of Aluminium Alloy

Aluminium Alloy	Values	Units
$Density$	2770	kg/m^3
$Poisson's Ratio$	0,33	$-$
$Young's Modulus$	7,1E+10	Pa
$Shear Modulus$	2,669E+10	Pa

As shown below in the Figure 3.6, in the CRM model a differentiation has been made in the body between the wing tip part, and the area closer to the wing root and the fuselage. This has been done in order to capture more reliably the deformation related to the wing tip, as well as to save on computational cost, since without this partition, the average cell size of the whole average would be much smaller, thus obtaining many more elements in the mesh. It is noteworthy that the fuselage in the structural part is of no interest, since it has been assigned the condition of "*fixed*" in the boundary conditions.

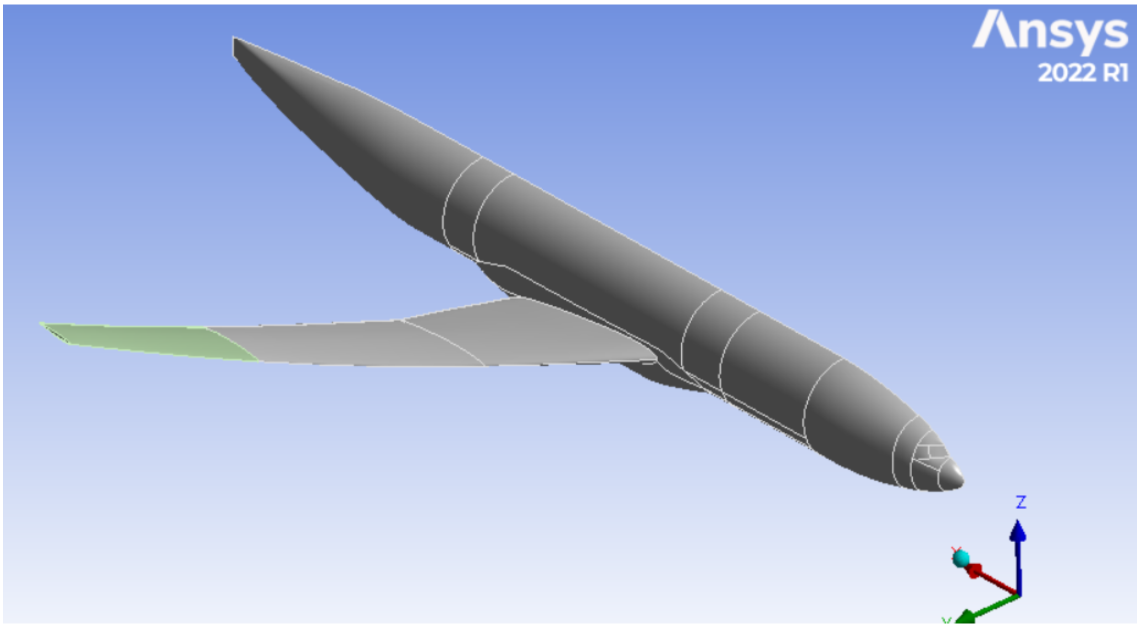

Figure 3.6: Wing-Body FEA model. Source: Own source

3.3.1 Structural mesh

According to mesh *ANSYS* recommendations, we have based on the most commonly used metrics – Skewness and Orthogonal Quality. It can be seen that low orthogonal quality and high skewness values are generally not recommended. Both metrics vary from 0 to 1.

Generally, it is recommended to keep minimum orthogonal quality value higher than 0.1, while maximum skewness less than 0.95. However, these values could be different depending on the physics and the location of the cell. These recommendations mainly concern meshes for CFD applications, and in general meshes for structural models are more permissive.

For that reason, we can find elements with a fairly high skewness value in the interface between the fuselage and root wing. But this does not cause any problems in the results, since, as mentioned above, the entire fuselage has a "fixed" condition. So it will not have any influence on the deformation results obtained.

As it is shown in the following Figure 3.7, differentiation has been made in the body between the wing tip part and the rest of the model. Obviously, the fuselage part is considered as "*fixed support*", so we can permit a much coarser mesh, as no displacement result is expected in this area.

On the other hand, in order to save computational resources, a differentiation has been made along the wing. Further refinement has been carried out on the wing tip part, with the aim of capturing more realistic deformation results and saving on computational cost. If the model were meshed with the same element size assigned to the wing tip, the total number of cells obtained would be too high and the computational cost would be too high. The difference grid refinement is shown in the Figure 3.8.

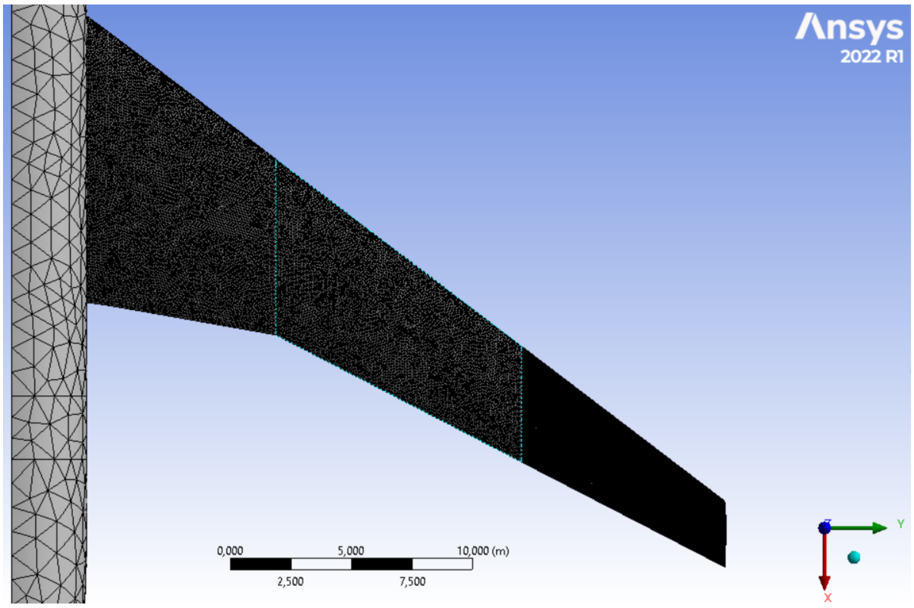

Figure 3.7: Wing-Body meshed model. Source: Own source

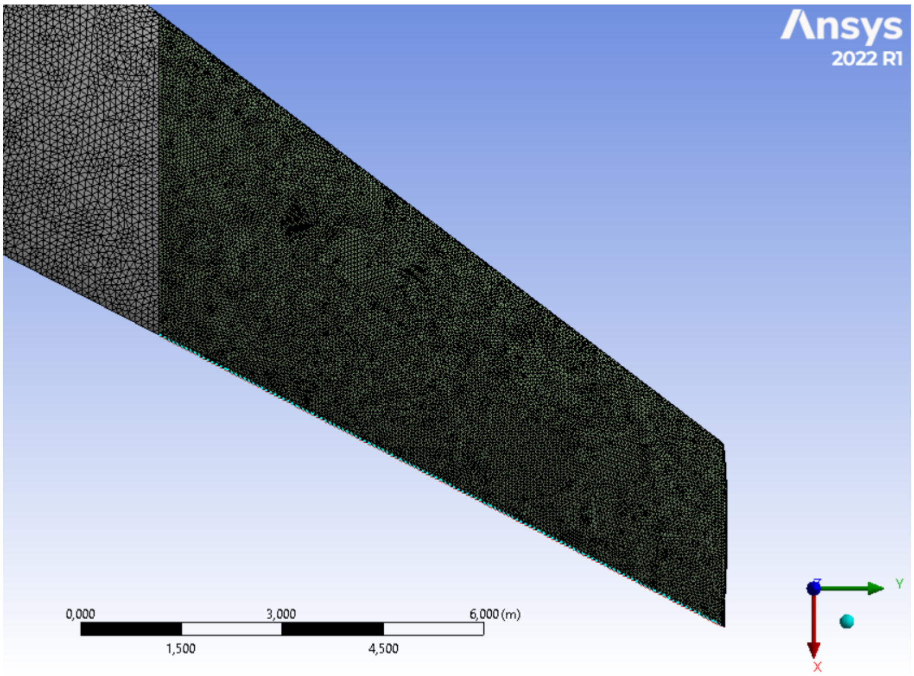

Figure 3.8: Wing tip refined mesh. Source: Own source

In addition, a mesh independence study has been carried out where three mesh refinements have been performed. All this in order to ensure that the wing displacement values are reliable and do not vary directly proportional to the mesh refinement. For the most refined grid 6.836.347 elements were used. Two coarser meshes were carried out by reducing each mesh size by 50 %, that is to say, 3.418.173 and 1.709.086 elements. The difference in the obtained values was less than 1 %.

4

Results

This section will present the results obtained in each and every one of the steps followed in the project.

When using CFD tools to understand the flows of aeronautical systems, we must first understand the characteristics of the flow. We must understand the reality on which we are going to validate the CFD code and processes.

The flow is mainly characterised by the Mach number. In the case of the present study, due to the requirements of the project, the flow has been established in a transonic regime, considering a Mach number equal to 0.85. The flow is also characterised by high Reynolds numbers that give rise to regions of laminar flow that become turbulent flow. Flows along the body and inlet surfaces create boundary layers, resulting in changes in the aerodynamic properties of the system. At transonic, supersonic and hypersonic speeds, shock waves are produced. Hence the importance of this study.

4.1 Verification study

The following study is conducted to demonstrate the accuracy of the CFD simulations so that they can be used with a minimum of confidence in aerodynamic simulation and the results can be considered credible so that the results can be taken into account and decisions based on it can be made in subsequent design.

To this purpose, in a fully autonomous way. The geometry has been downloaded and is available on the NASA website [26]. It is very important to note that it is a free source geometry (everyone has access) but it is not a plug-and-play model. This means that once downloaded, a preparation will be necessary to be able to perform further studies, both structural and CFD studies.

In order to verify the results obtained with those provided by the different references published on the NASA web site, different parameters have been studied at different Angles-of-Attack:

- Drag coefficient
- Lift coefficient
- Moment coefficient
- Pressure cofficient

4.1.1 General flow field

Under the general flow field conditions, the static pressure contour over the aircraft surface is generated in Figure 4.1. For the calculation of coefficients and their comparison with references, a Mach number of 0.85 has been considered. The static temperature of 310.92 K and a Reynolds number of $5 \cdot 10^6$ are set.

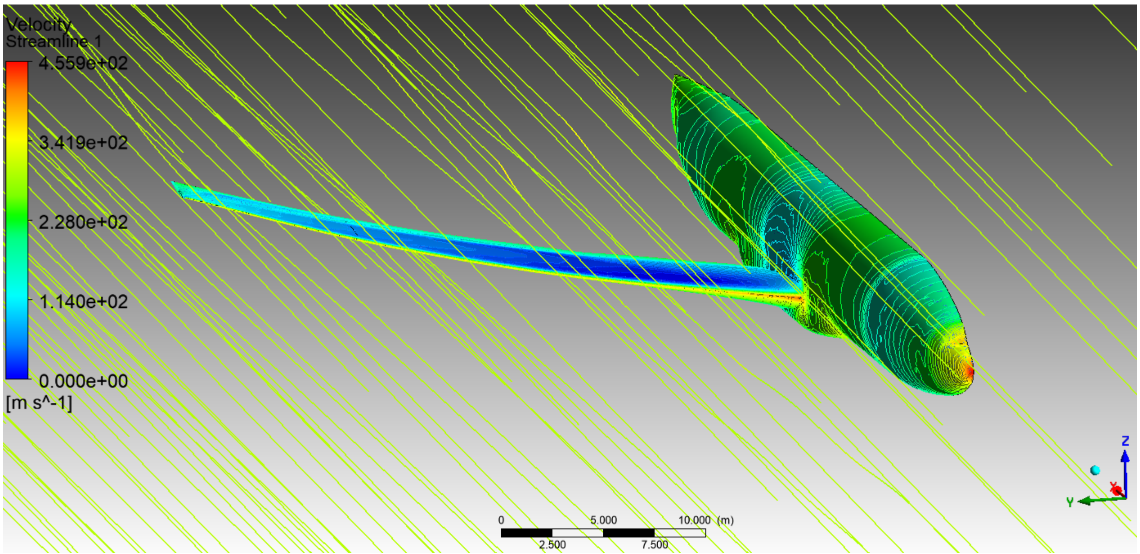

Figure 4.1: Flow field around the Common Research Model. Source: Own source

4.1.1.1 Comparison of Drag, Lift and Pitching moment

In the first instance, in order to validate a first simulation and carry out the coupled simulations, several coefficients have been studied to be sure that the initial conditions considered are correct.

The initial conditions with which the velocity and pressure values have been subsequently calculated are described in section 4.1.1. Different angles of attack (AoA) from 2,5º to 4º have been studied.

Different workshops [24] conducted by institutions and companies under the supervision of NASA have served as a reference to compare our results. In addition, the NASA CRM website [1] itself provides these results, so they will also be subject to comparison.

It is important to note that the references have used much more refined meshes, in the order of 10 times more. However, such computational power is not available for this project, so the size of the mesh elements has been reduced to minimum. In any case, the results obtained are really close.

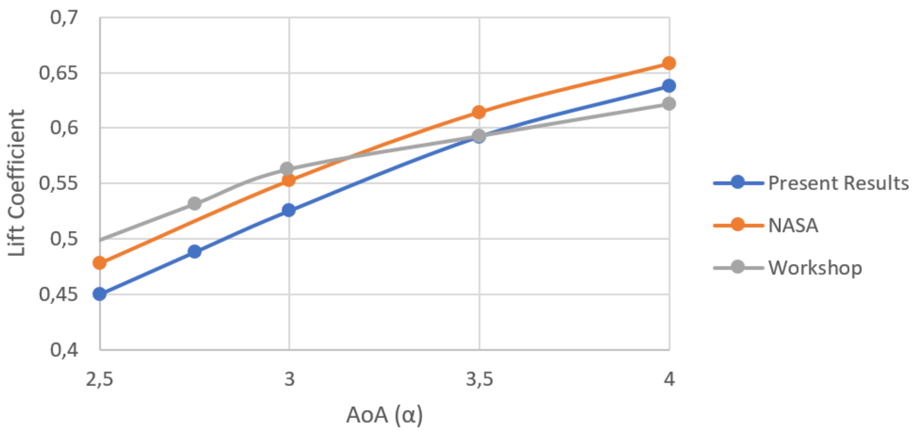

(a) Lift coefficient comparison

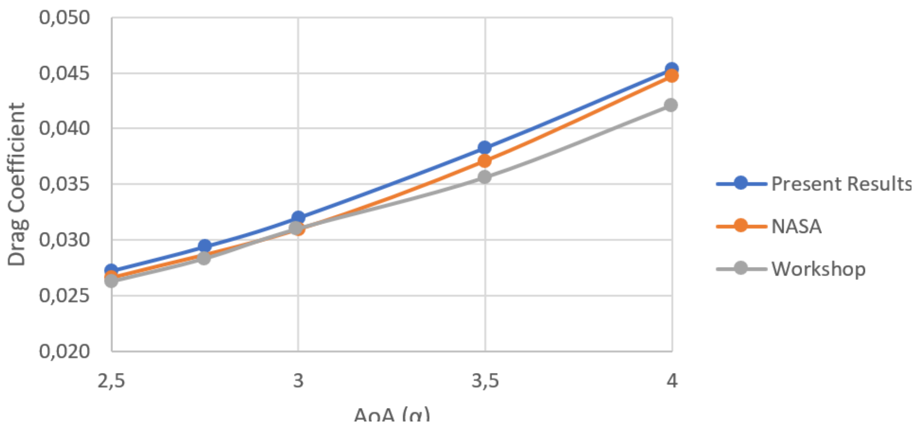

(b) Drag coefficient comparison

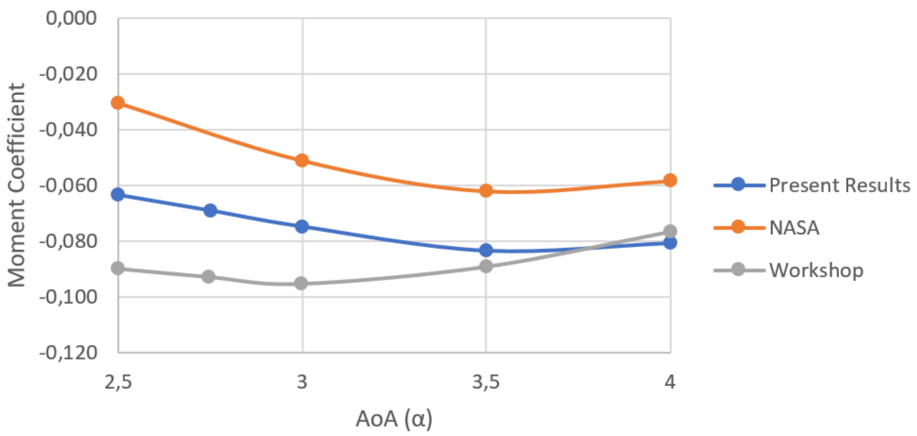

(c) Pitching moment coefficient comparison

Figure 4.2: Comparison of Lift, Drag and Pitching moment Coefficients. Source: Own source

As can be seen in Figures 4.2a, 4.2b and 4.2c, the results obtained are quite close to the references. For some angles of attack, some results differ to a greater extent than others, especially for smaller AoAs. This does not indicate that the computational results obtained are wrong, as we can see in Figures above how the results from the

Workshop and NASA itself also differ. With regard to simulations, they have been carried out with different mesh refinements. As there is no significant difference in the results, only the results for the mesh chosen as optimal in terms of time and accuracy of the results are shown.

4.1.1.2 Comparison of Pressure coefficients

In order to be absolutely sure of the quality of our results. A comparison of the pressure coefficient has also been carried out. A comparison of the pressure coefficient has also been carried out.

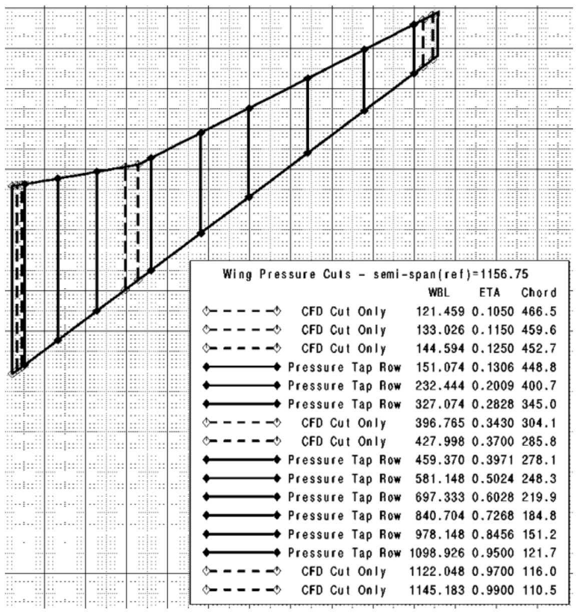

Figure 4.3: Wing Pressure Cuts - Semi-span locations. Source: [1]

It has been studied along the direction of semi-span. In figure 4.3 are shown the different semi-span locations considered. The comparison has been done for sections 4,6,9,10,12,14 and they are displayed in Figure 4.4.

As can be observed, the results are again really close to the benchmarks. So we could consider this first part of the study successful.

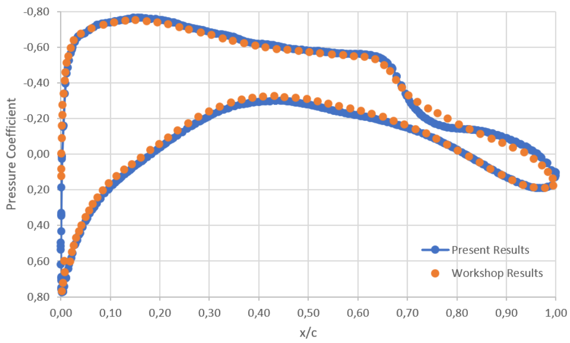

(a) η = 0,1306

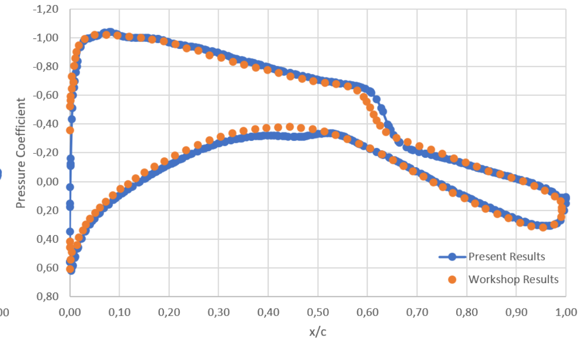

(b) η = 0,2828

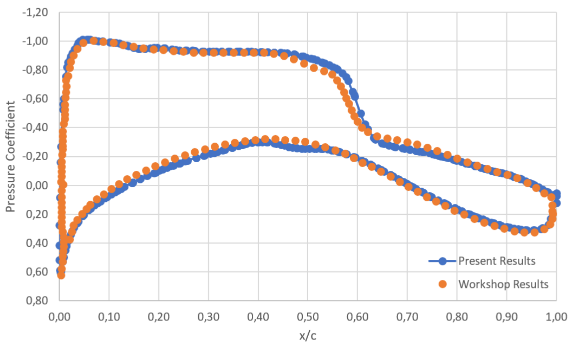

(c) η = 0,3971

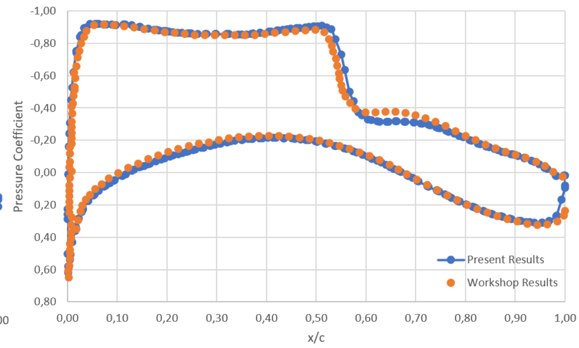

(d) η = 0,5024

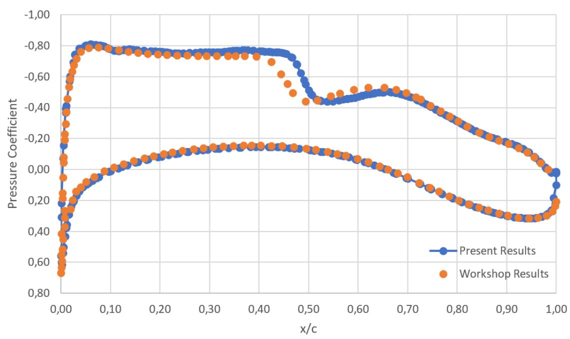

(e) η = 0,7268

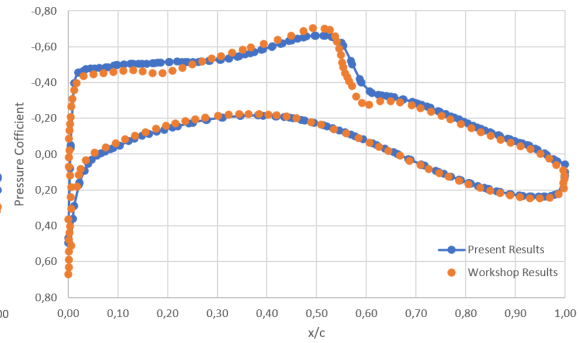

(f) η = 0,95

Figure 4.4: Comparison of Pressure Coefficients at different span locations for 2,75º AoA. Source: Own source

According to the explanation given in section 2.7.1, in Figure 4.4 can be observed the behaviour of the flow in terms of pressure over the different airfoils for the CRM Wing.

It can be appreciated how the pressure distribution is uniform between the leading edge and the shock wave formation, providing thus more lift even though the shock is weaker in comparison with conventional airfoils. Moreover, it can be observed the hight aft loading associated with higher cambered aft section.

4.2 One way simulation

4.2.1 Wing-Body Full scale simulation

4.2.1.1 Deformation for the Wing-Body Full Scale

In this section are provided the deformations results. Particularly, it is shown the vertical displacement of the wing. The simulations have been performed using two different materials. Firstly, the simulation have been done using Aluminium Alloy. The material properties of this Aluminium have been described in the Table 3.2.

On the other hand, Vascomax C250 was used according to the NASA workshop author. Vascomax C250 properties are show in the Table 4.1. The same results are not expected, as they took into account the internal structure of the model. However, this serves to validate the results to some extent.

In figures 4.5 and 4.7 are shown the images from the simulations. Finally, a comparative summary of the results is shown at 4.2.

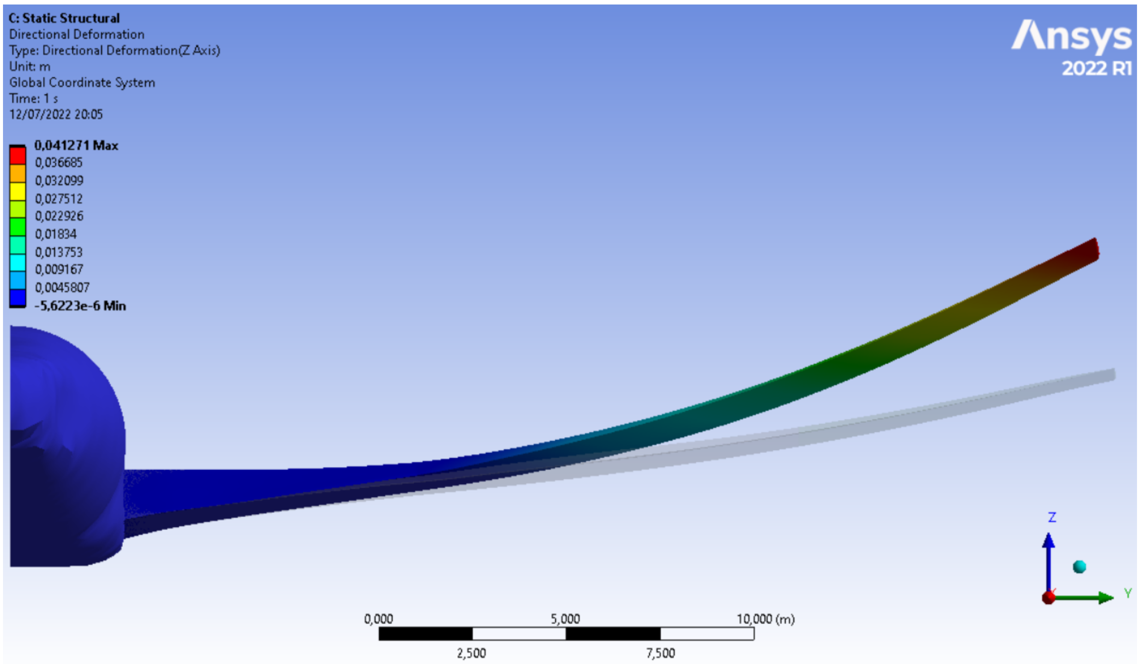

Figure 4.5: Total deformation from one-way simulations for Aluminium Alloy. Source: Own source

In the following figure 4.6 the comparison between the deformed and undeformed model is shown.

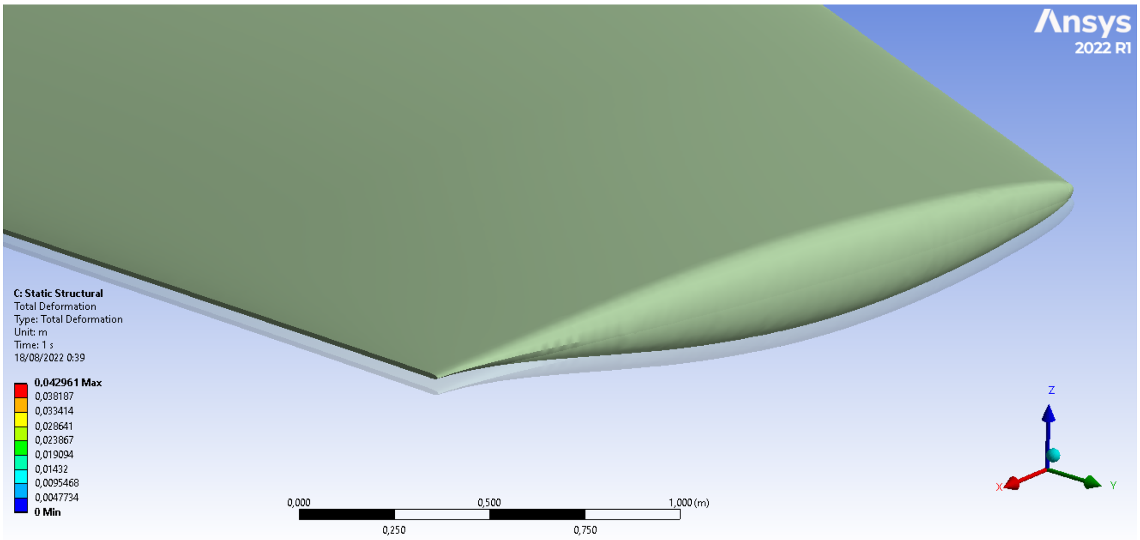

Figure 4.6: True scale (1.0) total deformation from one-way simulations for Aluminium Alloy. Source: Own source

Table 4.1: Properties of Vascomax C250

Vascomax C250	Values	Units
Density	4,581	kg/m^3
Poisson'sRatio	0,31	–
Young'sModulus	1,83E+11	*Pa*
ShearModulus	6,984E+10	*Pa*

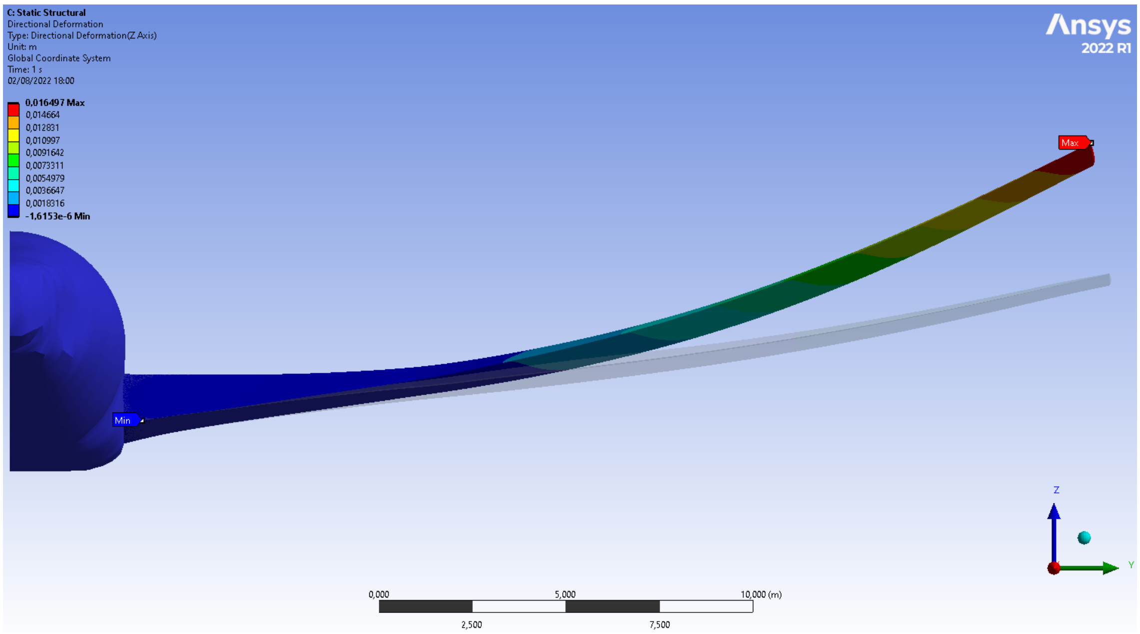

Figure 4.7: Total deformation from one-way simulations for Vascomax C250. Source: Own source

CRM Wing deformation		
Version	Displacement Value	Units
Aluminium Alloy	4,127	cm
Vascomax C250	1,649	cm
NASA Workshop	2,997	cm

Table 4.2: Vertical displacement of the wing in One-way simulations

Analysing the results, the wing formation values are not very significant. For the worst case in which aluminium is considered, the deformation value is about 4 centimetres. Taking into account that this is the full-scale model which has a semi-wingspan dimension of 29.38 metres, it is not a very significant deformation.

However, it would be interesting to analyse the pressure coefficients formed in the wing after deformation, in order to see the behaviour in the formation of shock waves.

4.2.1.2 Pressure

In order to perform the coupled simulation, it is necessary to transfer the pressure data from the flow field to the wing surface. The pressure transfer to the fuselage has not been taken into account, as it has been given the status of "*fixed support*" in the simulation and would therefore have no effect. At this point, it is important to ensure that all data points have been transferred to the surface.

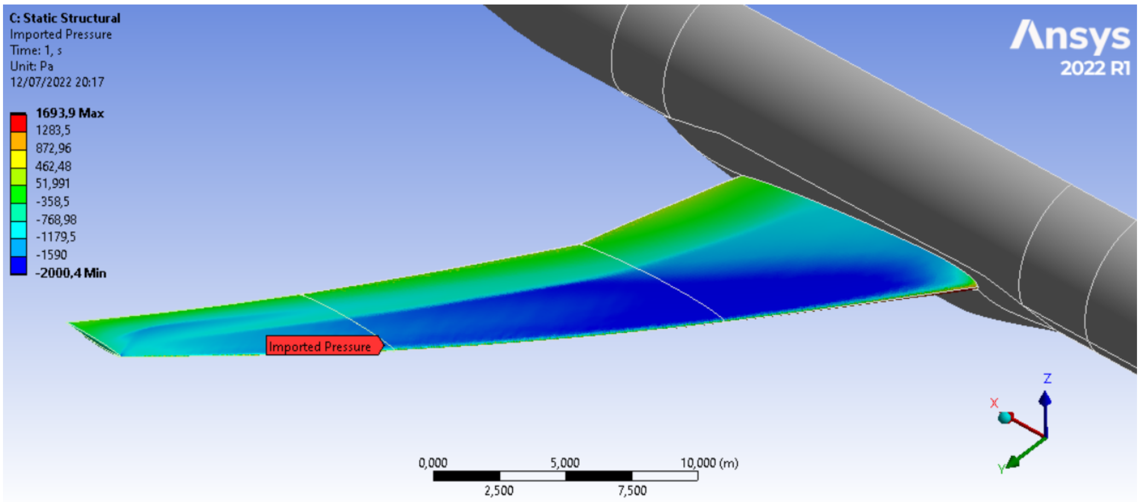

Figure 4.8: Imported pressure from Fluid field to upper wing surface. Source: Own source

In Figure 4.8, it can be observed that the blue region denotes the part of the wing which has a negative pressure that as one might expect, this is caused by the presence of the supersonic region (in which Mach number is higher than 1). Figure 4.9 shows the Mach number contour for section 4, where it can be seen that the supersonic region belongs to the red/orange zone. In this zone, the flow is accelerated and a lower pressure is generated. Once again, the concept of supercritical airfoil is referred in section 2.7.1, so the change from the blue region to the green region is characterized by the shock wave formation.

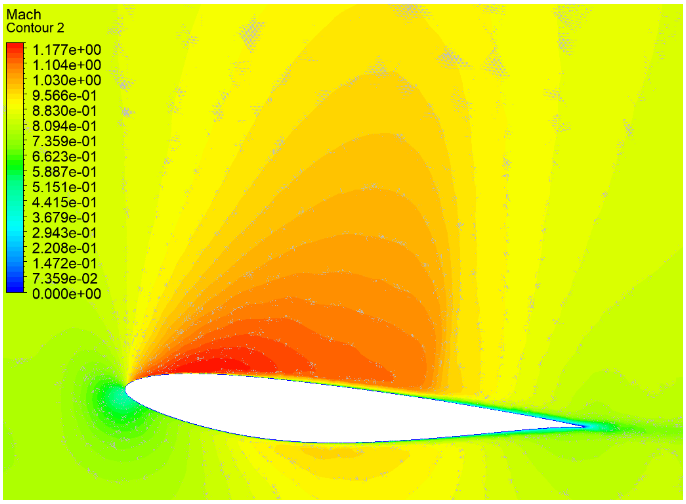

Figure 4.9: Mach Number contour for section 4 (η = 0,1306)

In figure 4.9, the mach number contour for the section 4 (η = 0,1306) is provide to show the shock wave formation over the upper surface, characteristic of this type of airfoil in transonic regimes.

4.2.2 Wing-Body 1/21 scale simulation

The study for the case of the tunnel scaled model (1/21) will help us to understand the behaviour of the model under the specific conditions described above. The aim of this study is to be able to have a computational model that describes in a sufficiently accurate way to be able to carry out further studies without depending on expensive wind tunnel experiments. Therefore, simulations have been carried out with different configurations in order to compare them with experimental data, which are not yet available.

The material Aluminium Alloy has been established for the whole model. In addition, the scaled model has the entire body filled, without internal structure.

4.2.2.1 Deformation for the Wing-Body 1/21 scale

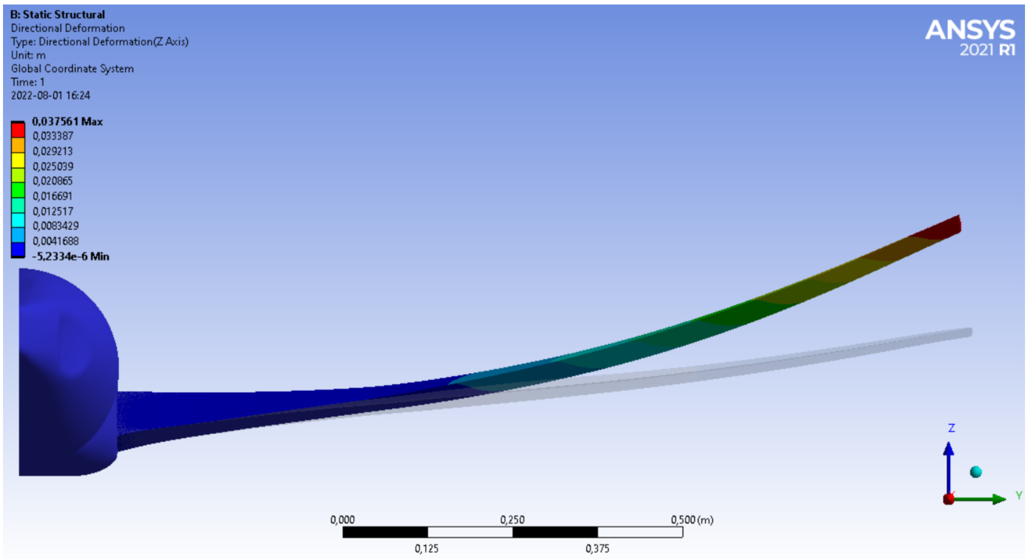

Figure 4.10: Total deformation from one-way simulations. Source: Own source

4.2.3 Wing-Body-Pylon-Nacelle 1/21 scale with engine ON

In order to obtain more realistic results, the WBPN model has been considered with the engine *ON*. In order to carry out this consideration, boundary conditions have been assigned on the engine surfaces. Specifically, on the Fan inlet and Fan outlet, assigning the conditions of *Pressure Outlet* and *Pressure Inlet*, respectively. In Figure 4.11 it is show the velocity contour to be able to see the effect of the assignment of these conditions.

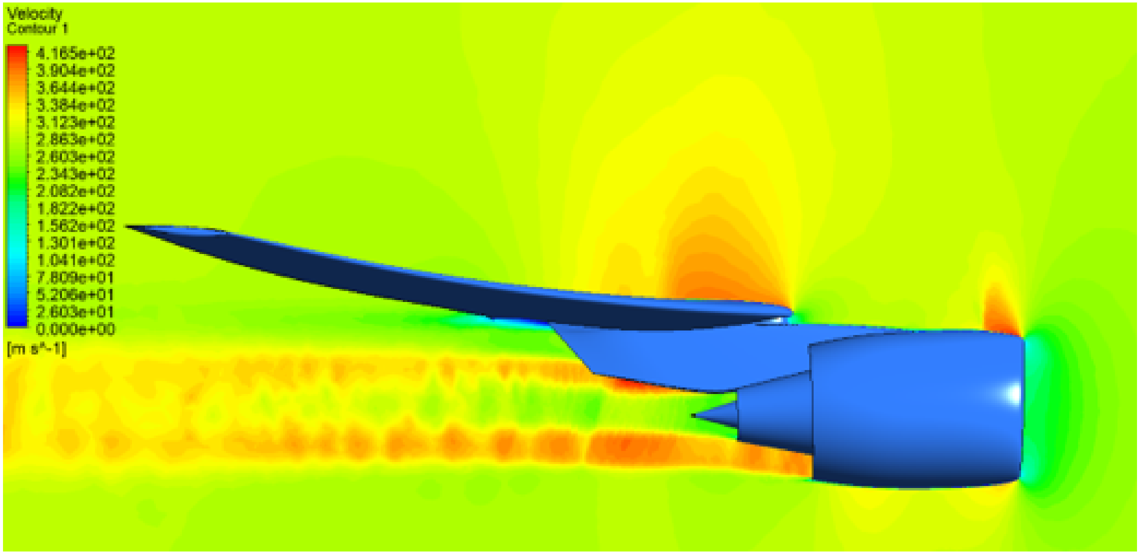

(a) Velocity contour for the mid-section of the nacelle

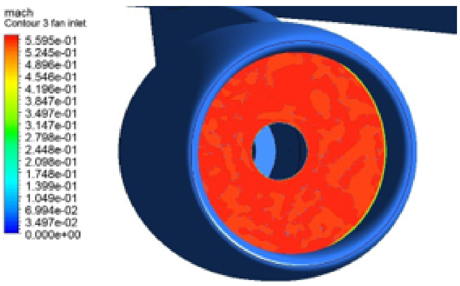

(b) Mach number contour for inlet fan surface

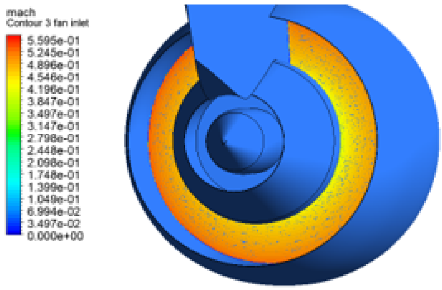

(c) Mach number contour for outlet fan surface

Figure 4.11: Velocity and Mach number contours for WBPN 1/21 scale model

4.2.3.1 Deformation for the Wing-Body-Pylon-Nacelle 1/21 scale

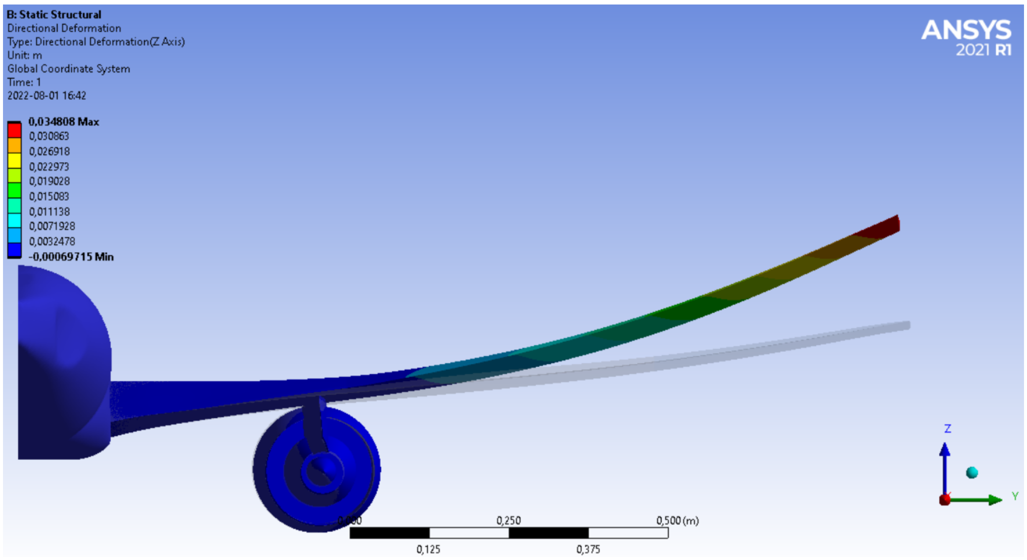

Figure 4.12: Total deformation from one-way simulations. Source: Own source

CRM Vertical wing deformation		
Configuration	Displacement Value	Units
Wing-Body	3,756	cm
Wing-Body-Pylon-Nacelle	3,480	cm

Table 4.3: Vertical displacement of the wing in One-way simulations

The difference in deformation values is very small between WB and WBPN (with engine ON) configurations. This is because the structural simulation has been carried out considering that the model is completely filled, as it is the 1/21 scale model used in the wind tunnel.

However, the explanation of why there is this difference must be given. First of all, and the most obvious, is that the WBPN has directly more weight due to the presence of the pylon and the nacelle, although it has only been simulated with the engine conditions on, this may be one of the causes. Moreover, the presence of the nacelle and pylon have important aerodynamic effects on the aircraft. In Figure 4.13, pressure coefficients at different span locations are provided for WB and WBPN (with engine ON) configurations. Clearly, it can bee seen how the absence of pylon and nacelle causes lower pressures in the upper surface of the wing leading to higher Lift values and, consequently, higher deformations.

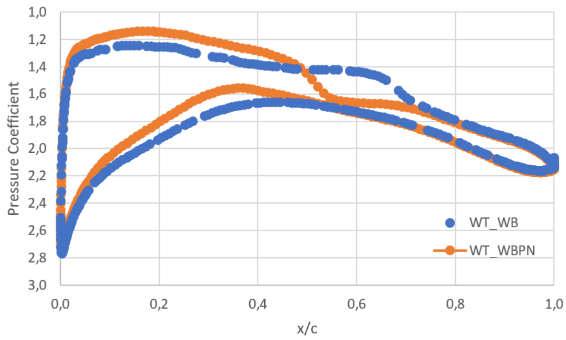

(a) $\eta = 0{,}1306$

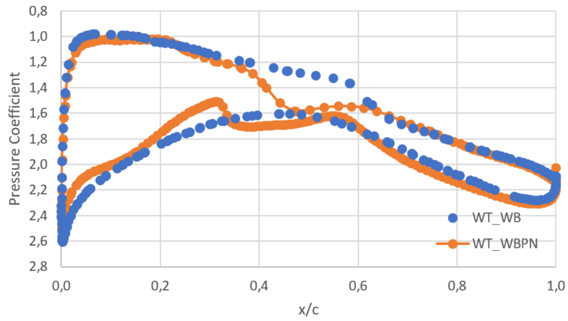

(b) $\eta = 0{,}2828$

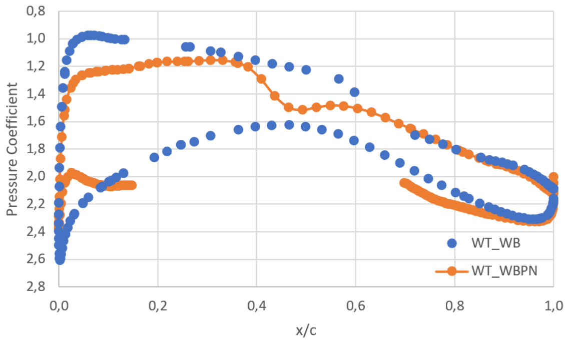

(c) $\eta = 0{,}343$

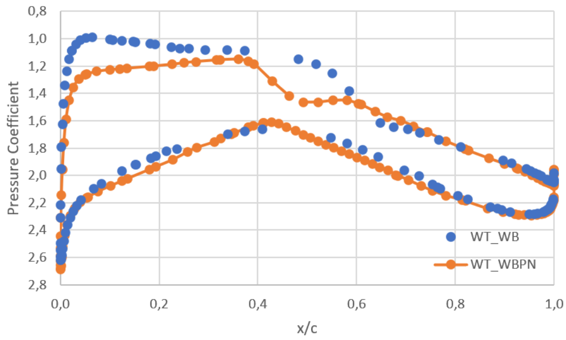

(d) $\eta = 0{,}3971$

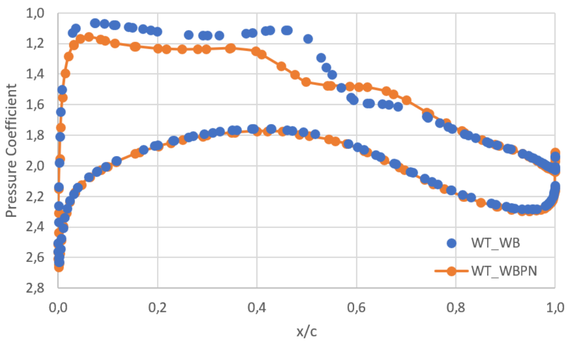

(e) $\eta = 0{,}5024$

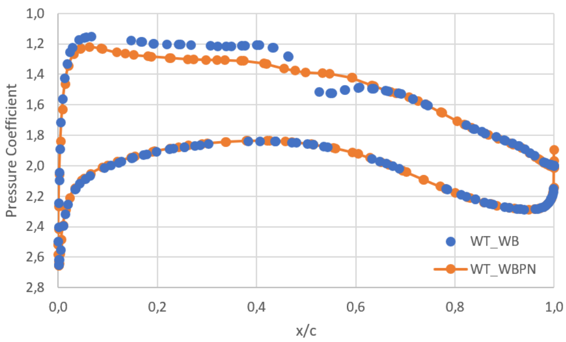

(f) $\eta = 0{,}7268$

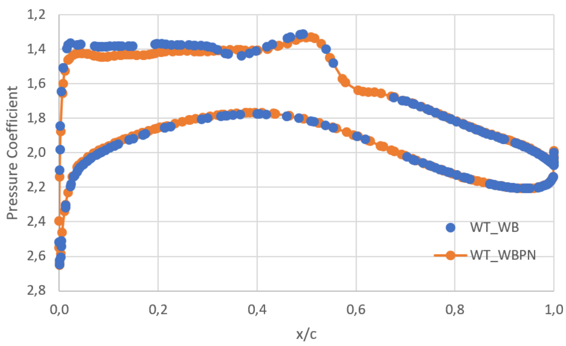

(g) $\eta = 0{,}95$

Figure 4.13: Comparison of Pressure Coefficients at different span locations between 1/21 scale WB and WBPN for 2,75º AoA. Source: Own source

In order to understand more clearly the above pressure coefficient charts at different spanwise locations, the transference of pressure to the wing surface (Figure 4.14) is interesting to see. In this manner, it is understood the delayed emergence of the shock wave along the chordwise for WB configuration.

At the final section the pressure coefficient graph becomes almost identical because the presence of the engine nacelle and the pylon have little effect on the aerodynamic behaviour at the wing tip.

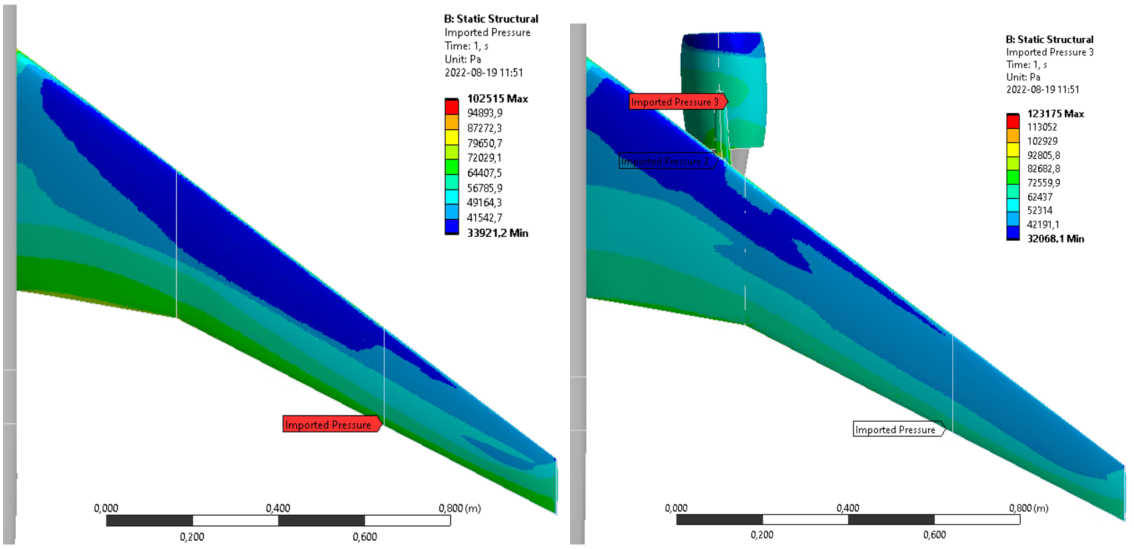

(a) Pressure transference to WB configuration

(b) Pressure transference to WBPN configuration

Figure 4.14: Static Pressure contour in the upper wing surface

4.3 Two way simulation

4.3.1 AGARD445.6 wing simulation

4.3.1.1 Modal study

In order to be in accordance with the literature related to the AGARD445.6 wing, a modal analysis study has been performed. The main reference for comparing the natural frequencies of the model is Yates (1987) [27]. In Figure 4.15, the results for the first four natural frequencies of the wing are shown, along with their mode shapes.

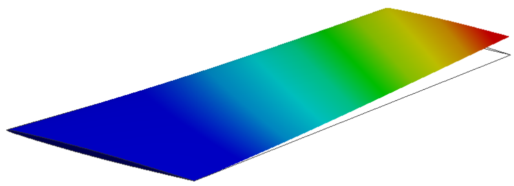

(a) 1st bending mode, f = 9,514 Hz

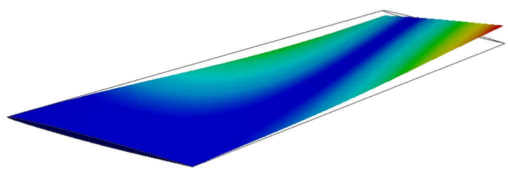

(b) 1st torsion mode, f = 40,316 Hz

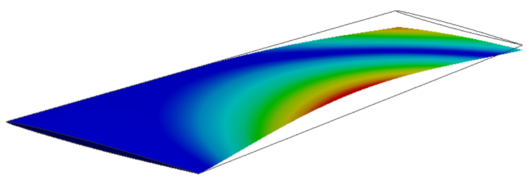

(c) 2nd bending mode, f = 49,614 Hz

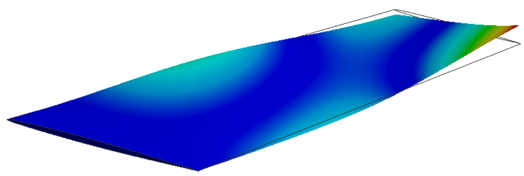

(d) 2nd torsion mode, f = 97,341 Hz

Figure 4.15: AGARD 445.6 mode shapes

The test model used in the experiments [27] was constructed by laminated mahogany, which has different material properties in each direction, i.e, It is an orthotropic material. The material properties which have been used are presented in the following Table 4.4.

Table 4.4: Properties of Laminated Mahogany

Laminated Mahogany	Values	Units
Density	397	kg/m^3
υ_{12}	0,31	–
υ_{13}	0,31	–
υ_{23}	0,31	–
E_{11}	3,1511	GPa
E_{22}	0,41621	GPa
E_{33}	0,41621	GPa
G_{12}	0,4392	GPa
G_{23}	0,4392	GPa
G_{13}	0,4392	GPa

Further on, in Table 4.5, a direct comparison has been made between different references already globally accepted in the scope of this study.

Solid Model	Mode 1 (Hz)	Mode 2 (Hz)	Mode 3 (Hz)	Mode 4 (Hz)
Yates (1987) [27]	9,60	38,10	50,70	98,50
Romanelli et al. (2010) [28]	9,57	39,28	50,35	93,63
Current	9,51	40,31	49,61	97,34

Table 4.5: Modal Frequencies for AGARD 445.6 Wing Model

As can be observed, the obtained results are very close to the cited references. Therefore, we can say that the results are correct in order to proceed with the study.

4.3.1.2 Structural Model

The structural model for the wing 445.6 was created in ANSYS. The assigned material is specified in the previous section in the Table 4.4.

The structure was meshed using a structure mesh using a total of 34276 elements. Different grids were used to achieve the closest modal analysis results with the minimum number of elements.

To receive the surface loads from the fluid flow, it is needed to specify a *Fluid Solid Interface* in the model. The AGARD445.6 wing was divided in different surfaces:

- Fluid Solid Interface

  Upper surface and Tip

  Bottom surface

- Fixed Support

  Root surface

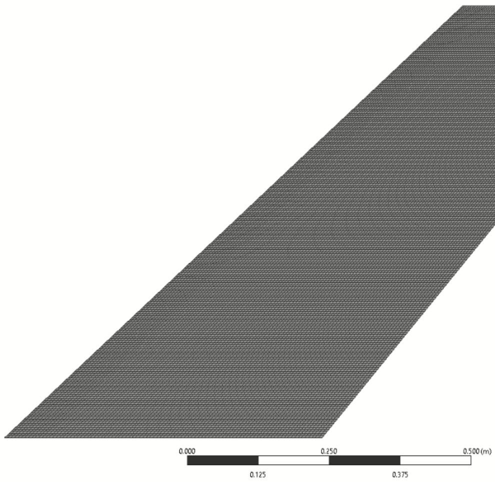

Figure 4.16: AGARD445.6 structural model. Source: Own source

4.3.1.3 Aerodynamic Model

The aerodynamic model for the AGARD445.6 wing was created in ANSYS Fluent. The software used to generate the mesh was ANSYS Meshing. On this occasion, an unstructured grid has been chosen due to its speed of generation. In addition, we wanted to try to carry out the study with a structured mesh, but because of various coupling problems between the structural solver and CFD, we finally went ahead with the unstructured mesh. The total number of fluid domain is 1.952.808 cells. Other more refined meshes were used to ensure the independence of the results. Due to the almost identical results, this mesh was continued.

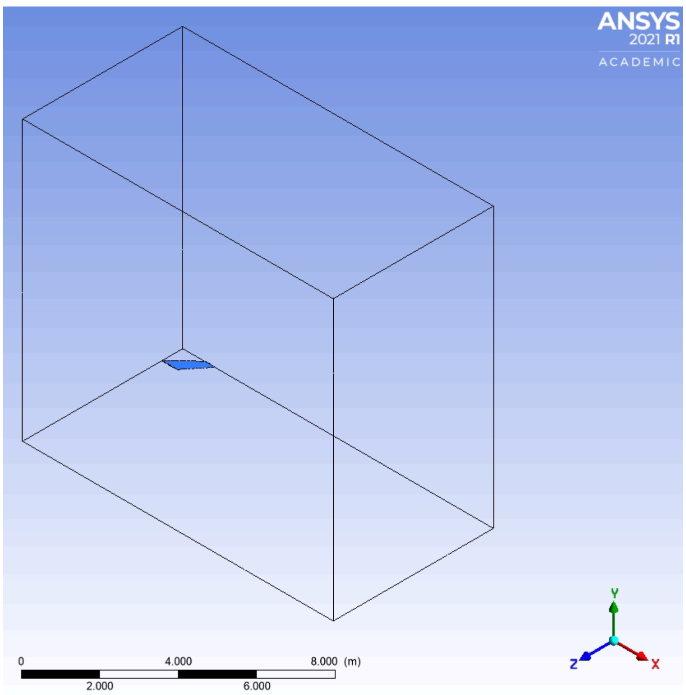

Figure 4.17: Agard fluid domain. Source: Own source

The boundaries of the domain that are open to fluid flow were defined as pressure far field boundary conditions; the wing surfaces (top, tip and bottom) were defined as "*no-slip walls*"; the wing root is attached to the "*symmetry*" wall. The mesh in the boundary layer of the wing was refined to reach a Y+ $\approx$ 1 in order to comply with the SST k-ω turbulence model grid constraints.

4.3.1.4 Results for Transonic Case

Before proceeding with the non-stationary simulation, steady-state simulations were carried out. This will serve as a first approximation of the wing surface pressure results, as well as an input for the transient simulation.

The results were computed at free-stream Mach of 0.96 for the AGARD445.6 wing model, considering the ideal-gas law for the air. In order to impose the static temperature in ANSYS Fluent, the experimental data were used. Moreover, according to references, a reynolds number of 526.600 was used based on MAC [28]. Regarding the boundary conditions, a pressure-far-field wall and an outlet-pressure were assigned.

In the simulations, the solver applied was the Pressure-Based, with a Courant number for the time-stepping scheme CFL equal to 5. Regarding the turbulence model that has been used, it was the SST k-ω.

As it has been mentioned before, before running the coupled simulations. Different grids were computed in order to achieve the closest results taking into account the pressure error and the computational time. It is important to remind that, this type of study requires a lot of computational resources and, for that reason, we are focused in this benchmark study and not in the CRM model. In Figure 4.18, the Pressure Coefficient contours can be observed between unstructured, structured (present results) and reference grid [28].

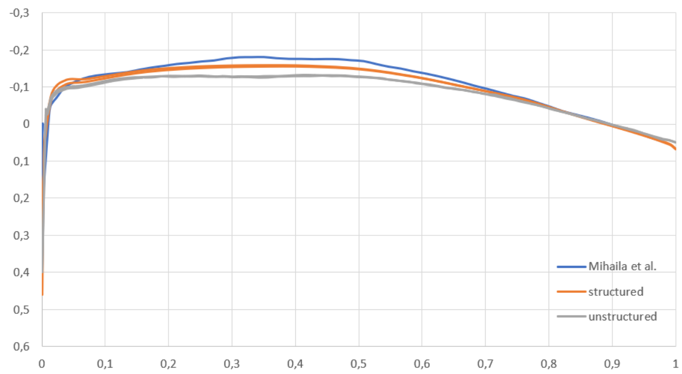

(a) 62.5% span location

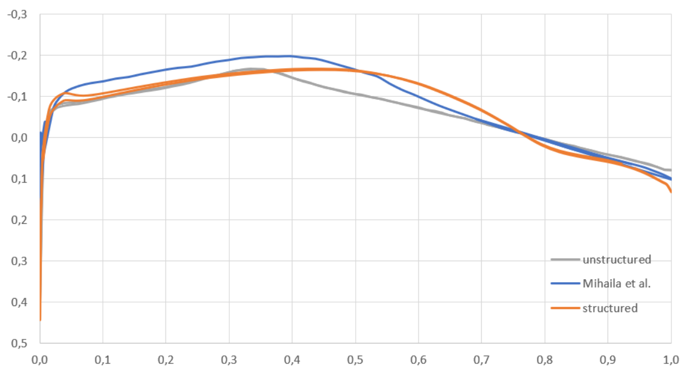

(b) 87.5% span location

Figure 4.18: Steady state pressure coefficient distributions at 62.5% and 87.5%

Simulation progress runs with a time step size of 0.001 seconds and different simulations have been performed at different velocities because we do not know exactly the moment when the wing starts to flutter. According to the reference, they have been performed a simulations in which the velocity is increasing from 305 m/s to 328 m/s [28]. To do this, it would be necessary to make a code for the speed to increase progressively. This activity is considered to be outside the scope of the project, so two main simulations have been carried out at different speeds.

Firstly, the coupled simulation is performed with an air velocity of 309 m/s. The behaviour of the leading and trailing edge displacement is shown in Figure 4.19. The simulation was performed up to 1.5 seconds, although only is shown up to 1 seconds. Clearly it can be seen that the displacement is following a damped behaviour. This explains why this speed turns out to be too low for the wing to start flapping.

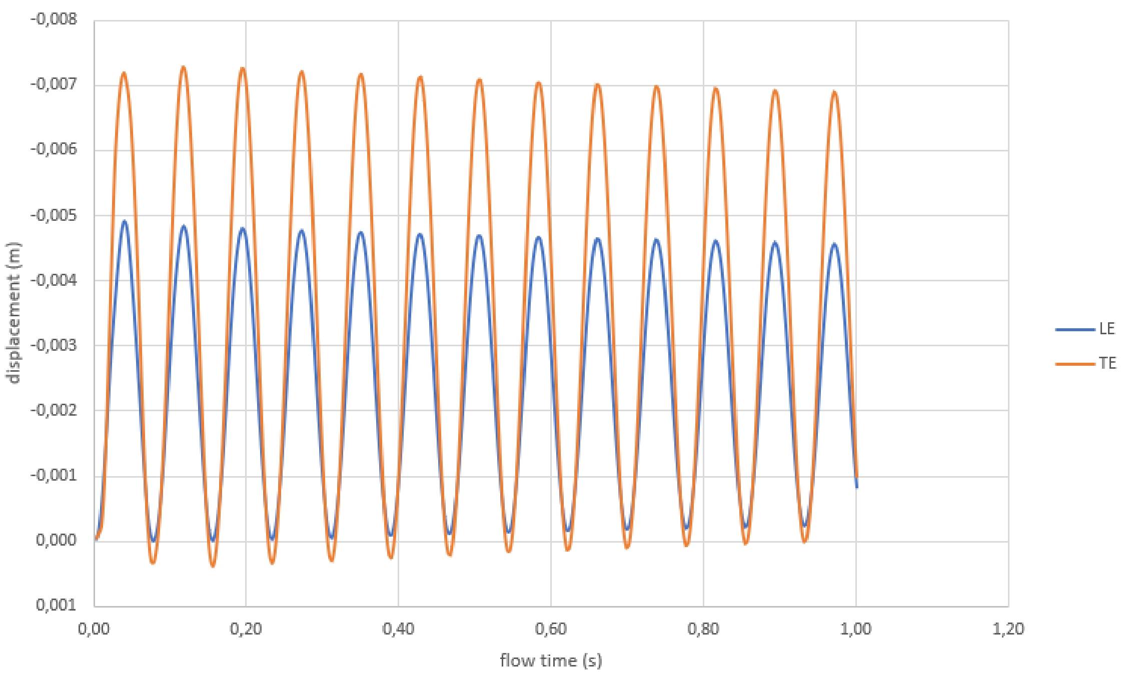

Figure 4.19: Wing leading edge and trailing edge tip displacement for Mach = 0.96, V = 309 m/s. Source: Own source

On the other hand, another simulation with an air velocity of 328 m/s was performed. In this case, in contrast to the previous one, the displacement of the leading and the trailing edge is diverging, so that it means that the AGARD445.6 wing starts to flutter from this velocity. This is in accordance with the reference with which the results are being compared [28]. Figure 4.20 shows the LE and TE displacement up to 1 seconds.

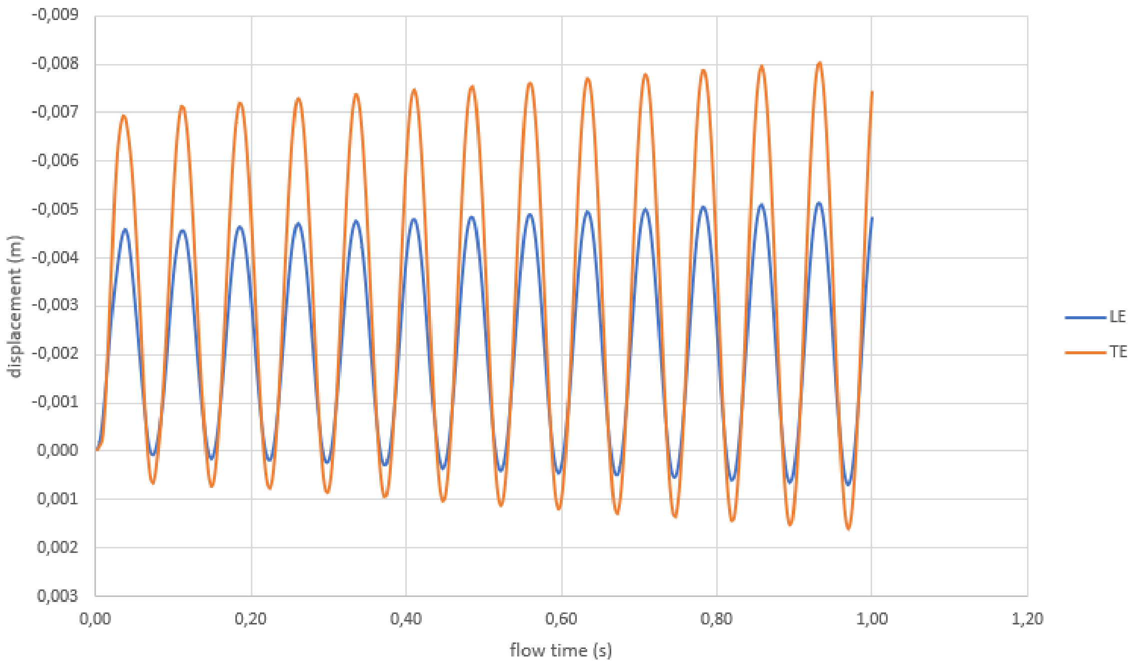

Figure 4.20: Wing leading edge and trailing edge tip displacement for Mach = 0.96, V = 328 m/s. Source: Own source

Apart from this, in Figure 4.21 is presented the flutter frequency analysis for the simulation with 328 m/s velocity considered.

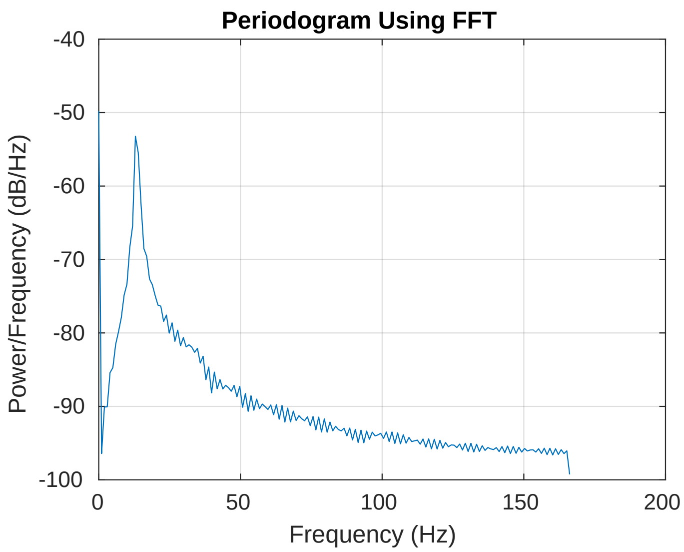

Figure 4.21: Flutter frequency, V = 328 m/s. Source: Own source

In agreement with the reference, the flutter frequency obtained in the results is very close to them. In the following Table 4.6 is presented the comparison:

References	Flutter Frequency
Romanelli et al. (2010) [28]	13.74 Hz
Current	12.93 Hz

Table 4.6: Flutter Frequency for AGARD 445.6 Wing Model for V = 328 m/s

It is important to highlight that different grid for CFD module have been used in order to ensure the independence of the results. A 40% more refined grid was tested. The results were very close to the initial grid. Moreover, in a coupled simulation is important to taking into account the effect of the time step size. Initially, a 0.002 seconds of time step was used, but the results differs when a 0.001 seconds time step was used. Then, in order to ensure the independence, a 0.0005 seconds was used, obtaining the same trend of displacement behaviour.

Finally, the work done in this benchmark can serve as a framework for future targeted research. Other parameters such as the influence on the study of the damping structure coefficient were also studied. The lack of information in the field for the software used has prevented a study on this.

5
Conclusion

5.1 Conclusion

In this thesis several results are provided with regard to aerodynamic coefficients and coupled simulation results for static and dynamic aeroelastic response. The aeroelastic studies have been performed through fluid-structure interation (FSI) of a Common Research Mode, using Ansys Fluent to compute the aerodynamic flow field and Ansys Structural to solve the structural deformation. NASA website [1] provides the geometry files to carry out the study. Nevertheless, the provided geometry needs to be prepared initially before starting the study due to errors found in the software used.

A first study in terms of initial verification of results has been carried out. This part has been done for the full-scale model of the CRM. It can be concluded in this part of the study that the results obtained are very close to the references used (both NASA itself, as well as the Workshops managed by it) [1] [24]. Results were obtained for the different aerodynamic coefficients: Lift, Drag, Pitching Moment and Pressure.

Secondly, in order to obtain a better understanding of the behaviour of the model used in the experimental wind tunnel simulations, the study has been carried out for the model scaled to 1/21. The model, in this case, is completely filled, as is the case for the model used in the experiments. Two configurations have been studied: WB and WBPN (with engine *on*). The boundary conditions for the 1/21 scale model have been provided by the project group. The same applies to the mesh independence study, so that the case could be used directly. Regarding the deformation values obtained in the static response study, they are in the order of 3-4 cm at the wing tip trailing edge, considering 2.4072º AoA. Moreover, by comparing the two configurations (WB and WBPN), the effect of the UHBPR nacelles on the pressure distribution on the wing surface is understood.

Finally, in relation to the dynamic aeroelasticity study. As mentioned throughout the document, it has unfortunately not been possible to reach our primary objective, the CRM, due to computational resources limitation. However, for this final part of the study, the AGARD445.6 wing has been used. At least this part, even if it is not the model of interest, is useful to understand the process of this type of study and the types of challenges involved. So, in one way or another, it serves as a framework for future projects in this field. Regarding the results obtained: Firstly, a modal analysis has been carried out in order to be in agreement with the published literature. In this case, it is a Two-way FSI simulation, so we have encountered the dynamic mesh challenge, which has been successfully carried out. In order to successfully carry out this study, a first verification of results with a steady-state simulation has been carried out. The pressure coefficients using different mesh types have been compared with the reference literature. The results of the dynamic response of the wing, as far as the wing tip deformations are concerned: 7mm for the trailing edge and 5mm for the leading edge. However, different behaviours are found at different flow velocities. For a speed of 309 m/s, the wing has a damped behaviour. While at 328 m/s, it presents a divergent behaviour, which suggests that it is in this case that the wing starts to flap. Finally, and also in agreement with the results mentioned above, a flutter frequency of 12.93 Hz is obtained, which is really close to the 13.74 Hz provided by the reference. For the Two-way simulation, apart from a mesh independence study, it is necessary to perform a time step size independence study.

After carrying out all these activities in the present project, there are many possibilities for future studies.

5.2 Future works

It is considered that, although very interesting results have been obtained for the understanding of the aeroelastic behaviour of the Common Research Model, this project is a first version that can be used to carry out future relevant work and research in the fields of aeroelasticity and aerodynamics.

In the first instance, a comparison of the deformation results obtained from the 1/21 scale model with the data obtained experimentally in the wind tunnel could be carried out. In addition, the values obtained from the one-way FSI analysis can be used to carry out a CFD simulation again to find out the effects of the deformation on the aerodynamic forces.

On the other hand, in order to obtain results on the dynamic response of the wing, it would be interesting to focus on optimising the case with as few cells as possible in the mesh. In this way, it would be possible to perform the Two-way FSI simulation of the Common Research Model wing. Or, alternatively, to carry out the same study with other software that is not limited by the available computational resources.

Finally, in order to obtain the closest results to reality, an important point would be to take into account the consideration of the internal structure of the wing, composed of spars and ribs. Although the model used for the experimental simulations in the wind tunnel is completely filled, this would give a better understanding of the aeroelastic behaviour of the real model. Apart from this, in the case where the engine is considered to be on (section 4.2.3), instead of assigning boundary conditions on the engine surfaces (fan inlet and fan outlet), the implementation of a body force model is considered to model the flow inside the nacelle and to increase the accuracy of the flow around the wing and to obtain a better understanding of the aeroelastic behaviour of the real model.

Bibliography

[1] NASA. *Common Research Model - High Speed CRM.* (accessed: 08.08.2022).

[2] Raymond L Bisplinghoff, Holt Ashley, and Robert L. Halfman. *Aeroelasticity.* Addison-Wesley series in mechanics. Addison-Wesley, 1955.

[3] Masashi Yamakawa and Kenichi Matsuno. “A Fluid-Structure Interaction Problem on Unstructured Moving-Grid using OpenMP Parallelization”. In: *Parallel Computational Fluid Dynamics 2006.* Ed. by J.H. Kwon et al. Amsterdam: Elsevier Science B.V., 2007, pp. 269–276.

[4] Jean-François Sigrist. “Fluid-Structure Interaction: An Introduction to Finite Element Coupling”. In: (Jan. 2015), pp. 1–283. DOI: 10.1002/9781118927762.

[5] *How Fluid-Structure Interaction Works and Why it’s Important.* https://www.ansys.com/blog/fluid-structure-interaction-explained. Accessed: 2022-05-30.

[6] Md.Fayaz Ahamed. “A Concise Description of One Way and Two Way Coupling Methods for Fluid-Structure Interaction Problems”. In: (May 2018).

[7] Björn Hübner, Elmar Walhorn, and Dieter Dinkler. “A monolithic approach to fluid-structure interaction using space-time elements”. In: *Computer Methods in Applied Mechanics and Engineering* 193 (June 2004), pp. 2087–2104.

[8] C. Michler et al. “A monolithic approach to fluid–structure interaction”. In: *Computers & Fluids* 33.5 (2004). Applied Mathematics for Industrial Flow Problems, pp. 839–848.

[9] Gene Hou, Jin Wang, and Anita Layton. “Numerical Methods for Fluid-Structure Interaction — A Review”. In: *Communications in Computational Physics* 12.2 (2012), pp. 337–377.

[10] Friedrich-Karl Benra et al. “A Comparison of One-Way and Two-Way Coupling Methods for Numerical Analysis of Fluid-Structure Interactions”. In: *Journal of Applied Mathematics* 2011 (2011), pp. 1–16.

[11] Inc. Release 12.0 © ANSYS. *26.1 Overview of Using the Solver.* URL: https://www.afs.enea.it/project/neptunius/docs/fluent/html/ug/node776.htm. (accessed: 12.02.2022).

[12] Wah Yen Tey et al. “Governing Equations in Computational Fluid Dynamics:Derivations and A Recent Review”. In: *Progress in Energy and Environment* 1 (2017), pp. 1–19.

[13] Jiyuan Tu, Guan Heng Yeoh, and Chaoqun Liu. *Computational Fluid Dynamics: A Practical Approach.* USA: Butterworth-Heinemann, 2007.

[14] John D. Anderson. “Governing Equations for Fundamental Aerodynamics”. In: *Encyclopedia of Aerospace Engineering* (Dec. 2010).

[15] L.Davidson. “An Introduction to turbulence models”. In: Course material (2003). DOI: 10.4208/cicp.291210.290411s.

[16] cadence-system analysis. *RANS*. URL: https://resources.system-analysis.cadence.com/blog/msa2021-the-reynolds-averaged-navier-stokes-rans-equations-and-models. (accessed: 06.07.2022).

[17] Simscale. *K-Omega and K-Omega SST*. URL: https://www.simscale.com/docs/simulation-setup/global-settings/k-omega-sst/. (accessed: 06.07.2022).

[18] cfd-online. *SST k-omega model*. URL: https://www.cfd-online.com/Wiki/SST_k-omega_model. (accessed: 06.07.2022).

[19] F. Menter. “Zonal Two Equation k-w Turbulence Models For Aerodynamic Flows”. In: *23rd Fluid Dynamics, Plasmadynamics, and Lasers Conference*. DOI: 10.2514/6.1993-2906. eprint: https://arc.aiaa.org/doi/pdf/10.2514/6.1993-2906. URL: https://arc.aiaa.org/doi/abs/10.2514/6.1993-2906.

[20] Iredia Erhunmwun and Usiosefe Ikponmwosa. “Review on finite element method”. In: *Journal of Applied Sciences and Environmental Management* 21 (Nov. 2017), p. 999.

[21] COMSOL-Multiphysics. *Analysis of Deformation in Solid Mechanics*. URL: https://www.comsol.com/multiphysics/analysis-of-deformation?parent=structural-mechanics-0182-192. (accessed: 08.07.2022).

[22] E.L. Houghton et al. “Chapter 8 - Airfoils and Wings in Compressible Flow”. In: *Aerodynamics for Engineering Students (Seventh Edition)*. Ed. by E.L. Houghton et al. Seventh Edition. Butterworth-Heinemann, 2017, pp. 525–573.

[23] A. Filippone (1999-2004). *High-Speed Aerodynamics: Supercritical Airfoils*. URL: https://aerodyn.org/supercritical/. (accessed: 31.08.2022).

[24] Inc. - Brian A. Edge Metacomp Technologies. *6th AIAA CFD Drag Prediction Workshop*. URL: https://aiaa-dpw.larc.nasa.gov/Workshop6/presentations/1_12_MetacompTechnologies.pdf. (accessed: 12.02.2022).

[25] Mohammad Keshavarzi, Aghil Yousefi-Koma, and Amir nejat. “One-way and Two-way Fluid-Structure Interaction Simulation and Analysis of a Wing”. In: Feb. 2016.

[26] NASA. *High speed CRM - Geometry*. URL: (https://commonresearchmodel.larc.nasa.gov/geometry/stp-files/). (accessed: 10.02.2022).

[27] E.C. Yates. *AGARD Standard Aeroelastic Configurations for Dynamic Response. Candidate Configuration I.-wing 445.6*. Defense Technical Information Center, 1987. URL: https://books.google.es/books?id=jCM2AQAAMAAJ.

[28] Mihai Mihaila-Andres, Constantin Rotaru, and Pericle Gabriel Matei. “Staggered Approach for Fluid-Structure Interaction Phenomena of an AGARD 445.6 Wing Using Commercial CFD/CSM Software”. In: *Journal of Aerospace Engineering* 28.4 (2015), p. 04014093.